TCAB1 is necessary for telomerase assembly

Basma S. Al-Masraf[1,2,3], Gloria I. Perez[1], Kate Adams-Boone[1], Scott B. Cohen[4], Li Han[5], Kefei Yu[5], and Jens C. Schmidt[1,6,✉]

[1]Institute for Quantitative Health Sciences and Engineering, Michigan State University, East Lansing, MI, U.S.A.
[2]College of Osteopathic Medicine, Michigan State University, East Lansing, MI, U.S.A.
[3]Cellular and Molecular Biology Graduate Program, College of Natural Sciences, Michigan State University, East Lansing, MI, U.S.A.
[4]Children's Medical Research Institute and University of Sydney, Westmead, NSW 2145, Australia.
[5]Department of Microbiology and Molecular Genetics, Michigan State University, East Lansing, MI, U.S.A.
[6]Department of Obstetrics, Gynecology, and Reproductive Biology, Michigan State University, East Lansing MI, U.S.A.

The ribonucleoprotein telomerase counteracts telomere shortening by adding repetitive sequences to the ends of human chromosomes. Telomerase is composed of the reverse transcriptase TERT, the telomerase RNA, and several auxiliary proteins that associate with the telomerase RNA, including TCAB1. TCAB1 is necessary for telomere maintenance in human cells and has been proposed to play a role in telomerase trafficking to Cajal bodies and telomeres, and in telomerase RNA folding. Here we show that, contrary to previous findings, TCAB1 is essential for telomerase assembly. We demonstrate that in the absence of TCAB1, the telomerase RNA is trapped in the nucleolus, a phase separated nuclear organelle, while TERT localizes to the nucleoplasm and is excluded from the nucleolus. Thus, nucleolar phase separation constitutes a barrier that counteracts telomerase assembly and TCAB1 is required to extract the telomerase RNA from the nucleolus, providing a molecular mechanism for the essential role of TCAB1 in telomerase function.

Telomerase | Telomere | TCAB1 | Telomerase Assembly | Liquid-Liquid Phase Separation | Cancer | Aging

Correspondence:
schmi706@msu.edu (Twitter: @jenscs83)

Introduction

Human chromosomes end in telomeres, which are long regions of repetitive double stranded DNA with a short single-stranded overhang (Stewart and Weinberg, 2006). Because the DNA replication machinery fails to copy the very end of the chromosome, telomeres shrink every time a cell divides (Harley et al., 1990). Eventually short telomeres trigger cell-cycle checkpoints that cause cells to enter senescence or to undergo apoptosis (Stewart and Weinberg, 2006). Telomere maintenance by telomerase is essential for continuous proliferation of stem cell populations in the human body and most cancers require telomerase activity for their survival (Stewart and Weinberg, 2006). To compensate for the incomplete replication of chromosome ends, telomerase appends TTAGGG repeats to the telomeric single-stranded overhang (Schmidt and Cech, 2015). Telomerase-mediated telomere maintenance requires three critical steps: Telomerase assembly, telomerase recruitment to telomeres, and telomeric repeat synthesis (Schmidt and Cech, 2015). Mutations in several genes have been identified that cause deficiencies in one of these critical steps and lead to a variety of diseases known as telomere syndromes (Armanios and Blackburn, 2012). In addition, telomerase is inappropriately activated in >85% of cancers (Stewart and Weinberg, 2006). While telomerase recruitment to telomeres (Nandakumar and Cech, 2013) and telomerase catalysis (Wu et al., 2017) have been studied extensively, much less is known about telomerase assembly. Importantly, telomerase assembly could be targeted to reduce telomerase activity in cancer cells, or to increase telomerase function in patients affected by genetically defined telomerase deficiency syndromes (Nagpal et al., 2020; Shukla et al., 2020).

Telomerase is a complex ribonucleoprotein (RNP). The core components of telomerase are the telomerase reverse transcriptase (TERT) protein, the telomerase RNA (TR), the H/ACA complex (dyskerin, NOP10, NHP2, GAR1), and the telomerase Cajal body protein 1 (TCAB1, also known as WRAP53) (Schmidt and Cech, 2015). The primary function of the H/ACA complex is to stabilize TR, by directly binding to its 3'-end preventing the exonucleolytic degradation of TR (Stuart et al., 2015; Tummala et al., 2015). The 3'-end formation of TR is tightly regulated by the competing activities of the poly-(A) polymerase PAPD5 and the nuclease PARN (Shukla et al., 2016; Tseng et al., 2015). In addition to TR, the H/ACA complex associates with a wide range of small nucleolar and small Cajal body-specific RNAs (snoRNAs and scaRNAs), which localize to nucleoli and Cajal bodies, respectively (Angrisani et al., 2014). Nucleoli and Cajal bodies are phase-separated nuclear organelles that play an important role in the biogenesis and maturation of variety of cellular RNAs, including components of the ribosome and spliceosome (Hyman et al., 2014; Mitrea and Kriwacki, 2016). TR is a scaRNA, which unlike snoRNAs contains a Cajal-body box (CAB-box) motif that associates with TCAB1 (Jády et al., 2004; Venteicher et al., 2009). An important function of TCAB1 is to drive exclusion of TR and other scaRNAs from the nucleolus and to facilitate their recruitment to Cajal bodies (Venteicher et al., 2009). In the absence of TCAB1, scaRNAs localize to the nucleolus (Venteicher et al., 2009). Therefore, TCAB1 controls which phase-separated nuclear organelle scaRNAs, including TR, are associated with.

Loss of TCAB1 function leads to telomere attrition in a variety of cell lines (Chen et al., 2018; Venteicher et al., 2009; Vogan et al., 2016; Zhong et al., 2011). In addition, several mutations in TCAB1 have been identified that cause misfolding of TCAB1 and lead to dyskeratosis congenita, a telomere syndrome (Freund et al., 2014; Zhong et al., 2011). While these observations highlight that TCAB1 is necessary for telomere maintenance, the underlying molecular mechanism is unclear. Initially, it was proposed that TCAB1 is required for telomerase recruitment to telomeres (Stern et al.,

2012; Venteicher et al., 2009). A more recent study suggested that TCAB1 is required for the correct folding of TR, and that its absence causes a reduction in telomerase activity (Chen et al., 2018). Importantly, all previous studies have come to the conclusion that TCAB1 is not required for telomerase assembly.

Here we analyze telomerase assembly in intact cells and by purification of the telomerase RNP and demonstrate that, contrary to previous findings, TCAB1 is required for telomerase assembly *in vivo*. Using a combination of genetic perturbations, biochemical analysis of telomerase function, cell biological approaches, and single-molecule live cell imaging, we show that in the absence of TCAB1, TR is sequestered in the nucleolus while TERT is excluded from the nucleolus. The spatial separation of TERT and TR that we observe in our experiments is inconsistent with proper telomerase assembly. Furthermore, we show that the limited amount of telomerase that can assemble in the absence of TCAB1 is fully active and can localize to telomeres, suggesting that TCAB1 is not required for the enzymatic function of telomerase or its recruitment to telomeres. In addition, we demonstrate that the diffusion properties of TERT in cells that lack TCAB1 closely resemble those of TERT that is not bound to TR. We conclude that the sequestration of TR in the nucleolus, when TCAB1 is absent, prevents its association with TERT, and that this lack of telomerase assembly is the molecular mechanism underlying the critical role of TCAB1 in telomere maintenance. Our results also demonstrate that the nucleolar phase separation constitutes a barrier for telomerase assembly and that TCAB1 is required to overcome it.

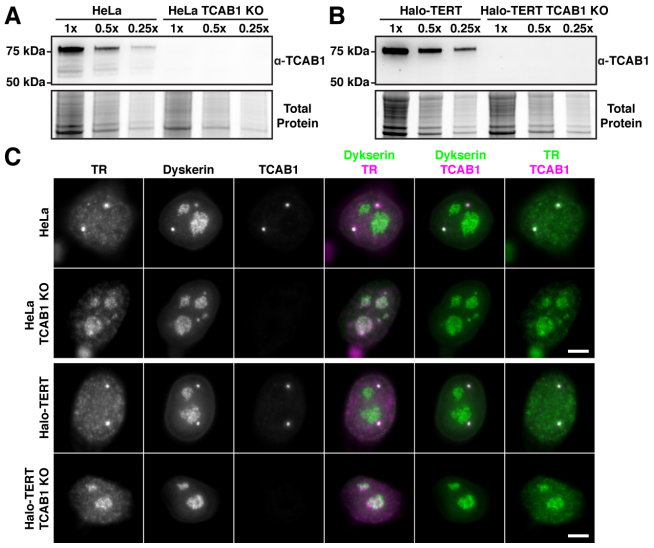

Fig. 1. TR is localized to nucleoli in TCAB1 knock-out cells. A-B Western blot demonstrating the absence of TCAB1 protein in TCAB1 knock-out cell lines generated from **A** HeLa and **B** Halo-TERT parental cell lines (probed with Proteintech TCAB1 antibody). **C** Immuno-fluorescence with anti-dyskerin and anti-TCAB1 antibodies coupled to fluorescence in-situ hybridization with probes against TR, demonstrating the absence of TCAB1 and TR localization to nucleoli in TCAB1 knock-out cells (scale bar = 5 μm).

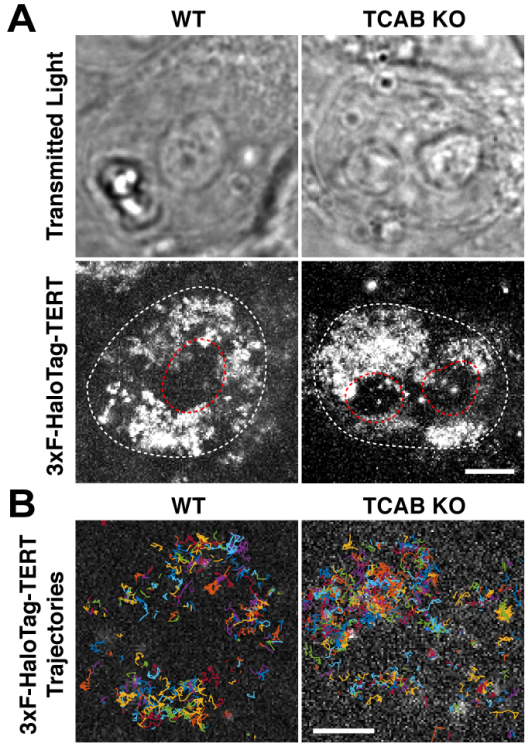

Fig. 2. TERT is excluded from nucleoli in control and TCAB1 knock-out cells. A Maximum intensity projections of 2000 frames of 3xFLAG-HaloTag (JF646) TERT movies (bottom), demonstrating that the TERT signal does not overlap with the nucleolus detected as circular shape in the transmitted light image in control and TCAB1 knock-out cells (top, red dashed line, scale bar = 2 μm). **B** TERT particle trajectories from the cells shown in Fig. 2A, demonstrating that TERT molecules move parallel to or away from the nucleolus when located at the interface between the nucleolus and nucleoplasm.

Results

Loss of TCAB1 leads to nucleolar accumulation of TR. To confirm that TR is sequestered in the nucleolus in the absence of TCAB1, we attempted to knock-out TCAB1 in parental HeLa cells and HeLa cells expressing 3xFLAG-HaloTag-TERT and mEos3.2-TRF2 from the endogenous *TERT* and *TRF2* loci (referred to as Halo-TERT from here on) using Cas9 and a single guide RNA targeting the first exon of the *TCAB1* locus (Fig. S1A). We isolated clonal cell lines that lacked a wild-type TCAB1 allele (Fig. S1B,C) and analyzed TCAB1 expression using Western blot. While a TCAB1 antibody targeting the N-terminus of TCAB1 failed to detect TCAB1 in our knock-out clones (Fig. S1D,E), antibodies raised against more C-terminal TCAB1 fragments detected a truncated form of TCAB1 (Fig. S1D,F,G). The size of the truncated TCAB1 is consistent with the use of methionine 129 as an alternative start codon. Importantly, the truncated form of TCAB1 localizes to Cajal bodies (Fig. S1H, arrows) and scaRNA localization is unaffected in its presence (Fig. S1I), indicating that it is at least partially functional. To avoid expression of the truncated TCAB1 variant, we knocked out TCAB1 using Cas9 with two guide RNAs to delete exons 2 and 3 from the TCAB1 gene, which removes the coding sequence for residues 144-214 of TCAB1 and results in a frame shift (Fig. S2A). TCAB1 knock-out was validated by Southern blot, PCR, Western blot, and immunoflu-

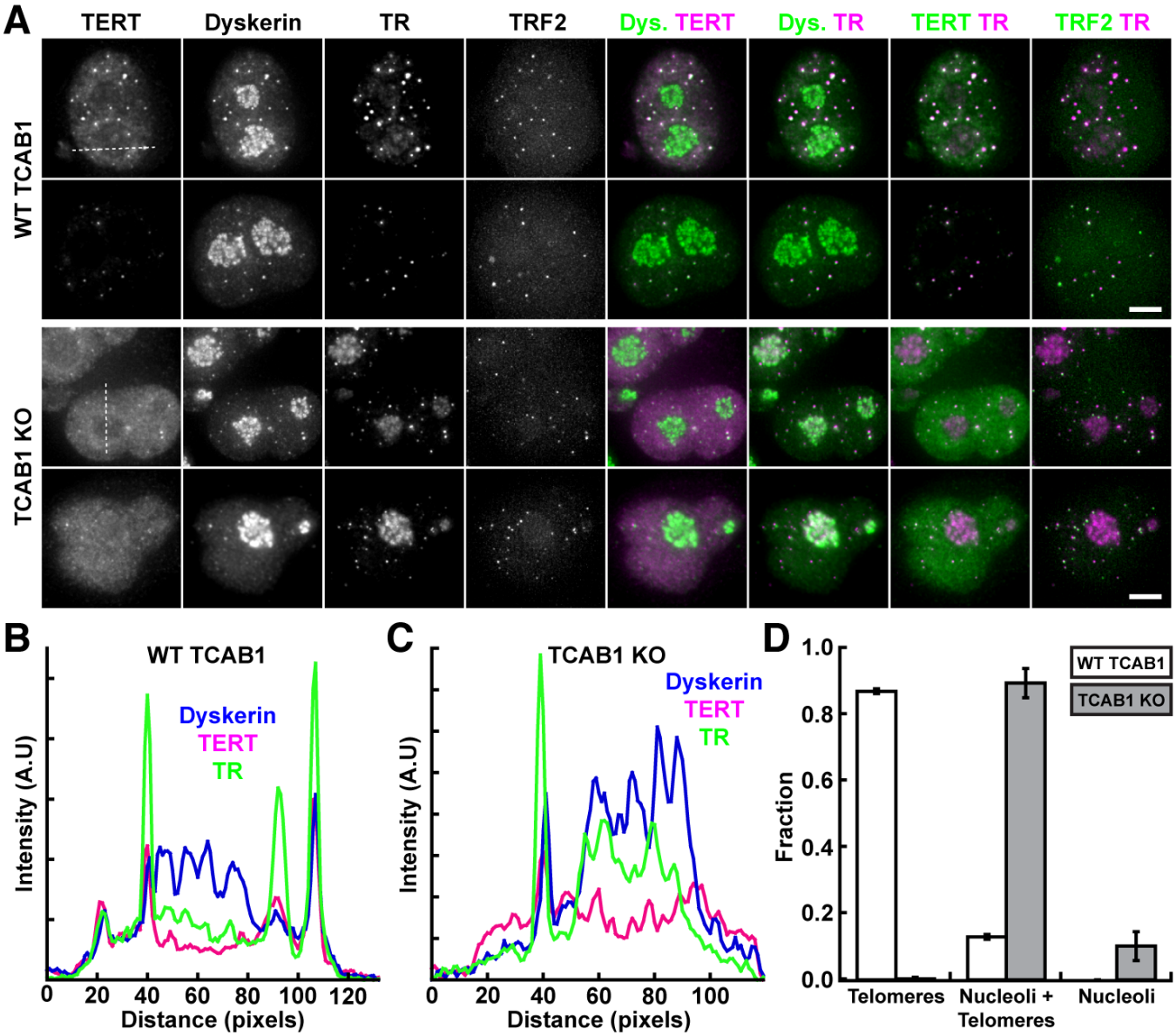

Fig. 3. TERT and TR localize to distinct nuclear compartments in TCAB1 knock-out cells. A IF-FISH images of control and TCAB1 knock-out HeLa cells (3xFLAG-Halo-TERT, mEOS3.2-TRF2) overexpressing mCherry-TERT and TR (scale bar = 5 μm). Cells were probed with antibodies against dyskerin and mCherry, and FISH probes specific to TR. The intrinsic fluorescence of mEOS3.2-TRF2 was used to detect telomeres. TR and TERT are co-localized at telomeres in control cells. In TCAB1 knock-out cells, TR is enriched in nucleoli, while TERT is depleted from nucleoli in both control and TCAB1 knock-out cells. Both TERT and TR also localize to telomeres in TCAB1 knock-out cells. **B-C** Line scans of **B** control and **C** TCAB1 knock-out cells along the dashed white lines in Fig. 3A, demonstrating the enrichment of TR (green) in nucleoli (blue) in TCAB1 knock-out cells and the depletion of TERT (magenta) from nucleoli in both control and TCAB1 knock-out cells. **D** Quantification of the fraction of cells showing TR localization exclusively to telomeres, to telomeres and nucleoli, or only to nucleoli in cells over-expressing mCherry-TERT and TR (3 independent experiments, >100 cells per experiments, mean ± standard deviation).

orescence imaging (IF, Fig. 1A-C, S2B,C). Fluorescence in situ hybridization (FISH) demonstrated that TR accumulates in the nucleolus in cells that lack TCAB1, as indicated by co-localization of TR and nucleolar dyskerin signals. This observation confirms that TCAB1 is required to extract TR from the phase separated nucleolus (Fig. 1C).

TERT is excluded from nucleoli. Our previous observations demonstrated that TERT does not enter nucleoli in human cancer cells (Schmidt et al., 2016). To confirm these results, we performed single-molecule imaging of 3xFLAG-HaloTag-TERT in living HeLa cells. Consistent with our previous results, 3xFLAG-HaloTag-TERT was not observed entering or overlapping with nucleoli, which are discernible as circular shapes in the nucleus under transmitted light illumination (Fig. 2A,B, Fig. S3A, Movie S1,2). TERT trajectories in close proximity to nucleoli revealed that their movement is biased away from the nucleolus, suggesting that TERT is repelled by the nucleolus (Fig. 2B). To exclude the possibility that nucleolar exclusion is a consequence of the 3xFLAG-HaloTag on the N-terminus of TERT used in our experiments, we transiently expressed the 3xFLAG-HaloTag fused to a nuclear localization sequence (NLS) in HeLa cells. Single-molecule imaging demonstrated that the nuclear 3xFLAG-HaloTag signals overlapped with the nucleolus (Fig. S3B,

Movie S3). Similar to the 3xFLAG-HaloTag alone, 3xFLAG-HaloTag-dyskerin also localized to the nucleolus (Fig. S3C). These results demonstrate that 3xFLAG-HaloTag-TERT is excluded from the nucleolus and that this exclusion is not caused by the 3xFLAG-HaloTag but instead is an intrinsic property of the TERT protein.

TERT and TR localize to distinct nuclear compartments in cells lacking TCAB1. It is well established that telomerase assembly is incomplete in human cancer cells, which leads to substantial pools of TERT and TR that are not assembled into telomerase RNPs (Xi and Cech, 2014). Together with our observation that TERT molecules rarely enter the nucleolus (Schmidt et al., 2016) this suggests that both free TERT and assembled telomerase RNPs do not enter the nucleolus. To test whether, like TR, TERT accumulates in the nucleolus in cells lacking TCAB1, we carried out single-molecule imaging of 3xFLAG-HaloTag-TERT. Strikingly, TERT localization is unchanged in cells lacking TCAB1 (Fig. 2A,B). This suggests that unlike TR, TERT does not accumulate in nucleoli when TCAB1 is absent. The experiments described so far demonstrate that TCAB1 is enriched in nucleoli and TERT is excluded from nucleoli in cells lacking TCAB1, but they do not simultaneously detect TERT and TR in the same cell. To overcome this limitation, we over-expressed mCherry-TERT and TR in TCAB1 knock-out cells. In controls, TERT and TR colocalized with dyskerin at telomeres marked by TRF2 (Fig. 3A). In addition, analysis of the TERT signal across the nucleus and nucleolus revealed that TERT was depleted from the nucleolus (Fig. 3B). Importantly, mCherry-dyskerin localized to the nucleolus, demonstrating that the mCherry-tag does not lead to nucleolar exclusion of its fusion partner (Fig. S4A). In cells lacking TCAB1, mCherry-TERT was diffusely localized in the nucleoplasm, localized to a subset of telomeres, and was depleted from the nucleolus (Fig. 3A,C). Similar to endogenous TR, overexpressed TR was enriched in the nucleolus in TCAB1 knock-out cells (Fig. 3A). In addition, TR was frequently co-localized with telomeres when mCherry-TERT and TR were overexpressed in cells that lack TCAB1 (Fig. 3A,C-D). Similar TR localization patterns were found when overexpressing untagged TERT and TR (Fig. S4B-C) and untagged TERT was excluded from nucleoli, confirming that nucleolar exclusion is an intrinsic property of TERT (Fig. S4D). Together these results demonstrate that, when overexpressed in TCAB1 knock-out cells, TR is enriched in nucleoli and TERT is depleted from nucleoli, consistent with a failure of nucleolar TR to assemble with TERT. In addition, our observations suggest that overexpression can partially overcome the sequestration of TR in the nucleolus when TCAB1 is absent, allowing a fraction of TR to bind to TERT and localize to telomeres.

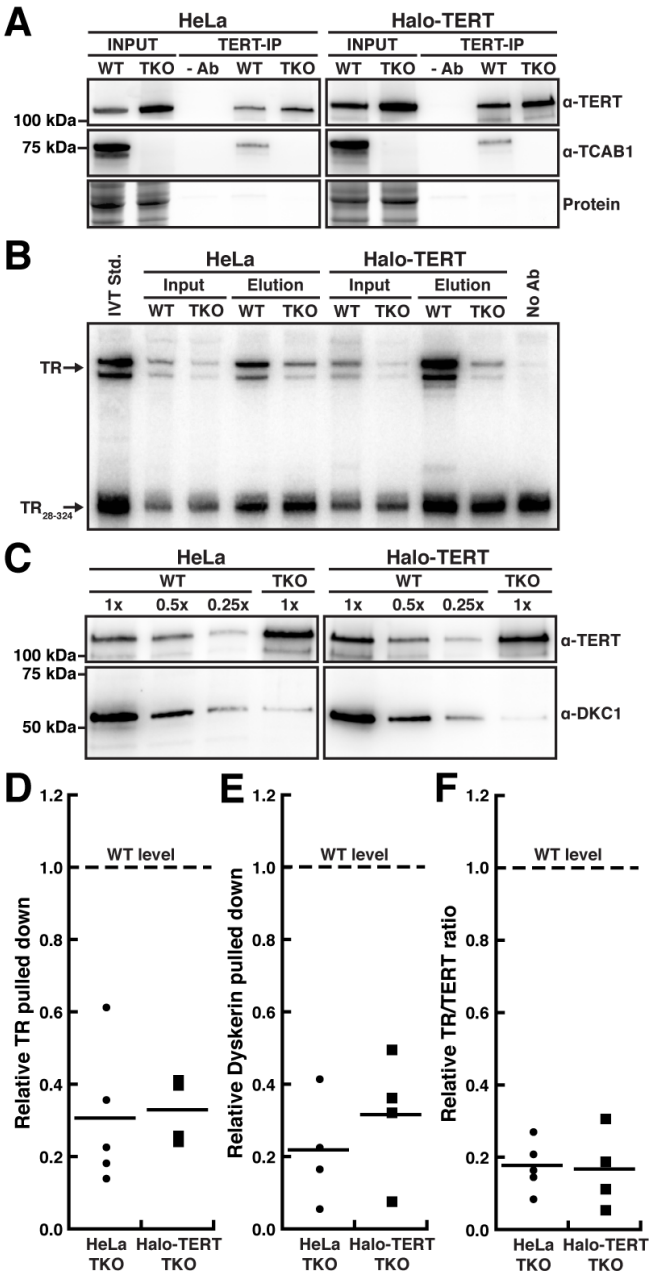

Fig. 4. Telomerase Assembly is reduced in the absence of TCAB1. A Western blots analyzing TERT immuno-purification (using a sheep anti-TERT antibody) probed with a rabbit anti-TERT antibody (Abcam) and a TCAB1 antibody. **B** Northern blot of RNA extracted from input and purified TERT samples probed with three radiolabeled DNA oligonucleotides complementary to TR. Standards are *in vitro* transcribed full-length TR and truncated $TR_{28\text{-}324}$. $TR_{28\text{-}324}$ was added to samples prior to RNA extraction as loading and recovery control. **C** Western blots to analyze immuno-purified telomerase RNP composition. A single membrane was cut into two pieces that were probed with TERT and dyskerin antibodies, respectively. **D-F** Quantification of the amount of **D** TR, **E** dyskerin, and **F** the ratio of TR to TERT in TERT purifications from TCAB1 knock-out cells compared to parental controls (n = 4-5, mean). The dashed lines indicate the level in telomerase purified from wild-type TCAB1 control cells which was normalized to 1.0.

TCAB1 is necessary for telomerase RNP assembly. Previous studies by other laboratories have concluded that telomerase assembly is unaffected by the absence of TCAB1 and whether TCAB1 is required for telomerase activity is controversial (Chen et al., 2018; Venteicher et al., 2009; Vogan et al., 2016). To assess the role of TCAB1 in telomerase assembly, we overexpressed TERT and TR in parental HeLa and TCAB1 knock-out cells and immuno-purified TERT using a well-established anti-TERT antibody (Cohen et al., 2007). To quantify telomerase assembly, we measured TERT levels by Western blot and determined the amount of TR co-

purified using Northern blot (Fig. 4A,B). The amount of TR associated with TERT purified from TCAB1 knock-out cells was significantly reduced compared to parental cells, for both HeLa (31 ± 9%, mean ± SEM, p = 0.001) and Halo-TERT (33 ± 4%, mean ± SEM, p = 0.001) cell lines (Fig. 4D). As a second measure of telomerase RNP assembly we quantified the amount of dyskerin associated with TERT (Fig. 4C). Since TR bridges TERT and dyskerin, dyskerin co-purified with TERT directly reports on the presence of TR. Consistent with the reduction in TR, the amount of dyskerin bound to TERT was also significantly reduced when purified from cells lacking TCAB1 compared to parental controls for both HeLa (22 ± 8%, mean ± SEM, p = 0.002) and Halo-TERT (32 ± 9%, mean ± SEM, p = 0.004) cell lines (Fig. 4C,E). Importantly, we also confirmed that TCAB1 is absent from telomerase purified from TCAB1 knock-out cells (Fig. 4A). As a final measure of telomerase assembly, we determined the ratio between TR and TERT (Fig. 4A,B,F), which was also significantly reduced when TERT was purified from TCAB1 knock-out cells (HeLa: 18 ± 3%, mean ± SEM, p < 0.001, Halo-TERT: 17 ± 5%, mean ± SEM, p < 0.001). Altogether, these results demonstrate that telomerase assembly is significantly reduced in the absence of TCAB1 and that overexpression of TERT and TR is not sufficient to overcome this defect in telomerase RNP formation.

TCAB1 is not required for telomerase catalytic activity. Previous work by others has suggested that the defects in telomere maintenance observed in TCAB1 knock-out cells are the consequence of reduced telomerase activity caused by the miss-folding of the telomerase RNA rather than impaired telomerase assembly (Chen et al., 2018). This TR folding model predicts that the specific activity of telomerase is reduced. To determine the specific activity of telomerase purified from TCAB1 knock-out cells, we measured telomerase activity using the direct telomerase extension assays (Fig. 5A,B, S5), and divided the activity by the amount of TR in the respective telomerase sample (Fig. 4B,D), which is a direct measure of the quantity of telomerase RNP present. Total activity of telomerase purified from TCAB1 knock-out cells was significantly reduced relative to telomerase purified from parental controls telomerase (HeLa: 24 ± 6%, mean ± SEM, p < 0.001, Halo-TERT: 34 ± 9%, mean ± SEM, p = 0.005), consistent with observations by others (Chen et al., 2018). In contrast, the specific activity of telomerase derived from cells that lack TCAB1 was not significantly reduced compared to controls (HeLa: 90 ± 9%, mean ± SEM, p = 0.35, Halo-TERT: 76 ± 10%, mean ± SEM, p = 0.1). Together these observations suggest that TCAB1 is required for telomerase assembly and that the limited amount of telomerase RNP that can form in the absence of TCAB1 is fully active.

TCAB1 is required for telomerase assembly in living cells. The experiments presented thus far demonstrate that telomerase assembly is significantly reduced in the absence of TCAB1 but were carried out in fixed cells or cell lysates. To analyze telomerase assembly in intact cells, we

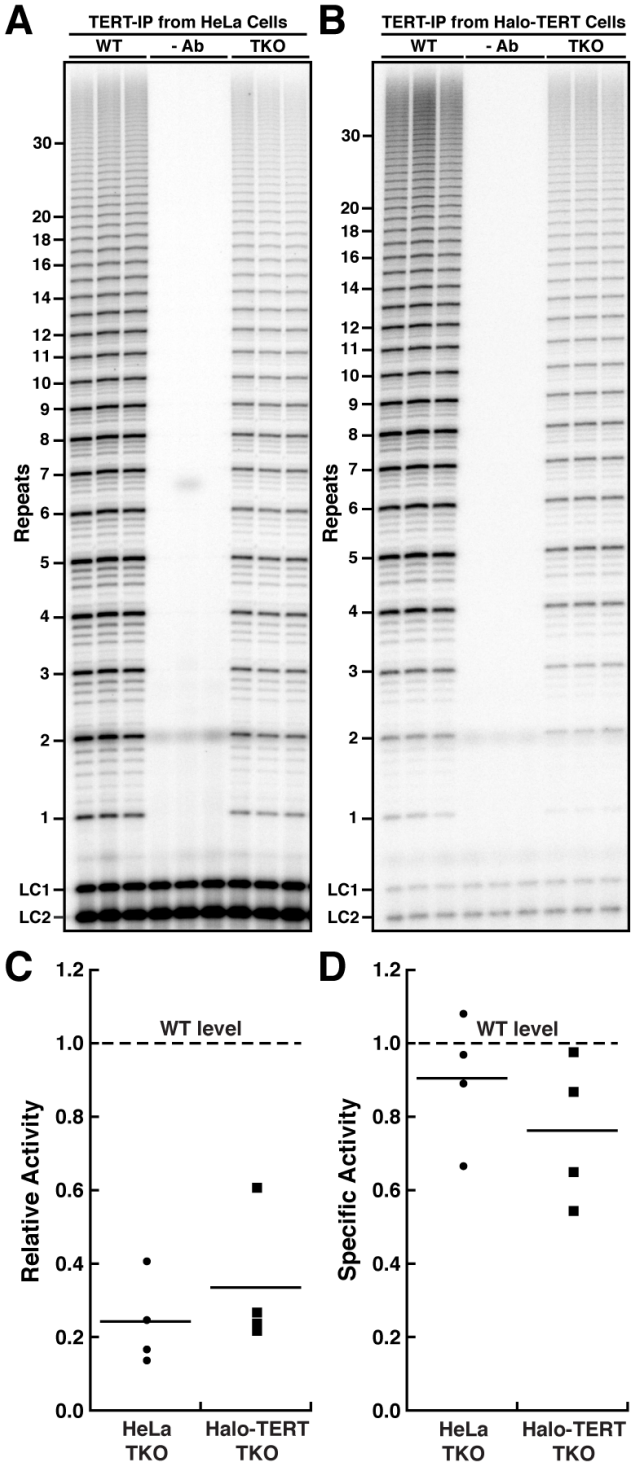

Fig. 5. The specific activity of telomerase is unchanged in the absence of TCAB1. A-B Direct telomerase extension assay of telomerase immuno-purified from parental (WT) and TCAB1 knock-out (TKO) **A** HeLa and **B** Halo-TERT cell lines. LC1 and LC2, radiolabeled DNA oligonucleotide loading controls. In -Ab samples the TERT antibody was omitted during the immuno-purification. **C** Quantification of telomerase activity in samples from TCAB1 knock-out cells relative to parental controls (n = 4, mean). **D** Specific activity of telomerase purified from TCAB1 knock-out cells relative to parental controls (n = 4, mean). Specific activity was calculated by dividing the relative activity (see Fig. 5C) by the relative amount of TR present in immuno-purified TERT samples (see Fig. 4D). The dashed lines indicate the activity level in telomerase purified from wild-type TCAB1 control cells which was normalized to 1.0.

carried out live cell single-molecule imaging of 3xFLAG-HaloTag-TERT and determined the diffusion coefficient of TERT particles (Fig. 6A, Movie S4, Fig. S6E). The diffusion co-efficient is a measure of the rate of movement of a molecule and depends on the size of the complex it is part of and reports on molecular interactions formed with other sub-cellular structures. Analysis of the diffusion coefficients of TERT trajectories in control cells revealed three distinct populations of TERT particles (Fig. 6B-D). A static population (D_S = 0.03 μm^2/s, 12%) which likely represents assembled telomerase RNPs bound to telomeres or Cajal bodies, a slowly diffusion population (D_{F1} = 0.35 μm^2/s, 28%) and a rapidly diffusing population (D_{F2} = 1.54 μm^2/s, 60%). The slowly diffusing population likely includes assembled telomerase RNPs, while the rapidly diffusing particles represents TERT molecules, which are not assembled with TR (Fig. 6B). Importantly, these diffusion coefficients are largely consistent with our previous results using a distinct method to determine their values (Schmidt et al., 2016). In the absence of TCAB1, the diffusion coefficient of the freely diffusing TERT population was increased (D_{F2} = 1.78 ± 0.04 μm^2/s, mean ± SEM, p = 0.04, Fig. 6C) and the fraction of the TERT populations that includes assembled telomerase RNPs was significantly reduced ($F_{Slow+Static}$ = 29 ± 1%, mean ± SEM, p = 0.02, Fig. 6D). This observation is consistent with our model that in the absence of TCAB1 telomerase assembly is defective. To determine the degree to which telomerase assembly is affected in cells lacking TCAB1, we knocked out TR, completely abolishing telomerase assembly. TR knock-out was confirmed by PCR and Sanger sequencing, FISH, and qPCR (Fig. S6A-C). Similar to control cells and TCAB1 knock-out cells, TERT was also excluded from nucleoli in cells lacking TR (Fig. S6D). Strikingly, the diffusion coefficients and the fraction of slow and static TERT particles in cells lacking TR closely resembled those of TCAB1 knock-out cells (Fig. 6A-D, S6D Movie S4-5). To analyze the interaction of TERT with telomeres, we filtered out TERT trajectories that came into proximity with telomeres marked by mEOS3.2-TRF2, as previously described (Schmidt et al., 2016). To assess the interaction of TERT with telomeres, we plotted the step-size vs. the distance from the closest telomere for each step of these trajectories (Fig. S7A). In control cells, we observed an enrichment of smaller step sizes and particles in close proximity to telomeres, consistent with TERT interactions with the telomere (Fig. S7A). In contrast, TERT trajectories from TCAB1 knock-out cells lacked this enrichment, and the step size vs. distance from the closest telomere plots were identical to those from TR knock-out cells (Fig. S7A). In addition, diffusion analysis using SpotOn revealed that the fraction of static TERT particles at telomeres was were reduced from 12% in control cells to 4-5% in TCAB1 and TR knock-out cells (Fig. S7B). These observations indicate that in the absence of either TCAB1 or TR, stable interactions of telomerase with telomeres occur at a lower frequency because they require base pairing of TR with the chromosome end (Schmidt et al., 2018). Together these results demonstrate that telomerase assembly is strongly reduced in the absence of TCAB1.

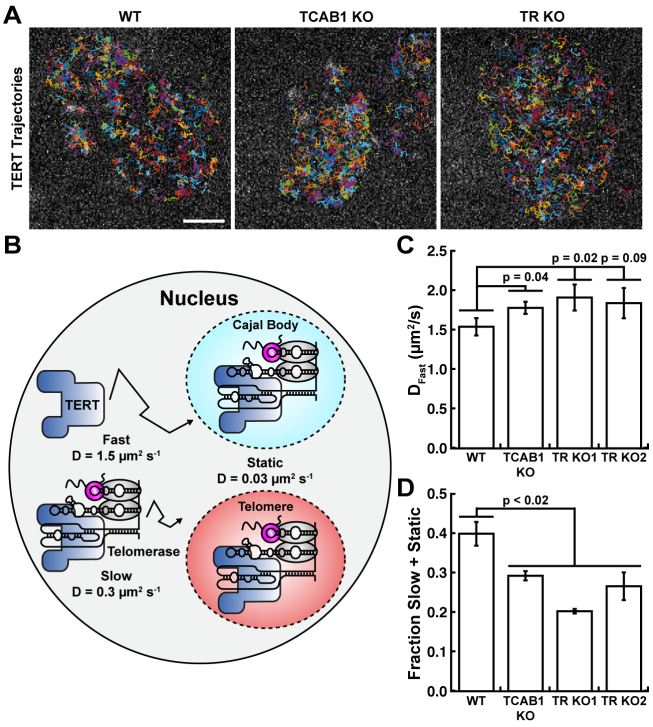

Fig. 6. TERT and TR do not assemble into telomerase in TCAB1 knock-out cells. A TERT particle trajectories from control, TCAB1 knock-out, and TR knock-out cells expressing 3xFLAG-HaloTag TERT (JF646, scale bar = 2 μm). **B** Diagram of distinct populations of TERT particles detected in control cells. **C** Diffusion co-efficient of the rapidly diffusing TERT population in control, TCAB1 knock-out, and TR knock-out cells (3 independent experiments, >15 cells per experiment per cell line, mean ± standard deviation, complete data in Fig. S6D). **D** Fraction of slow plus static TERT particles in control, TCAB1 knock-out, and TR knock-out cells expressing 3xFLAG-HaloTag TERT (3 independent experiments, >15 cells per experiment per cell line, mean ± standard deviation, complete data in Fig. S6D).

Discussion

The experiments described in this study demonstrate that TCAB1 is necessary for telomerase assembly. In the absence of TCAB1 the telomerase RNA is targeted to the nucleolus via its association with dyskerin and other components of the H/ACA complex. In contrast to TR, TERT cannot enter the nucleolus, preventing its association with TR in cells that lack TCAB1. In addition, we demonstrate that sequestration of TR in the phase-separated nucleolus in the absence of TCAB1 can be partially overcome by telomerase overexpression, leading to telomerase assembly and localization to telomeres. This suggests that the nucleolus has a limited capacity to accommodate cellular RNAs and that TCAB1 is not required for telomerase recruitment to telomeres. Finally, we demonstrate that while telomerase assembly is limited the specific activity of telomerase is unchanged in the absence of TCAB1, which excludes a role of TCAB1 in telomerase catalytic function. Altogether our work completely reshapes our understanding of the role of TCAB1 in telomerase function in human cells and demonstrates that nucleolar phase separation is a barrier counteracting telomerase assembly.

The importance of TCAB1 for telomere maintenance is undisputed (Chen et al., 2018; Venteicher et al., 2009).

Knock-out or depletion of TCAB1 results in telomere shortening (Chen et al., 2018; Venteicher et al., 2009; Vogan et al., 2016). All previous work also concluded that TR is enriched in the nucleolus in the absence of TCAB1 (Chen et al., 2018; Stern et al., 2012; Venteicher et al., 2009; Vogan et al., 2016; Zhong et al., 2011). Finally, all prior studies propose that TCAB1 is not required for telomerase assembly but instead plays a role telomerase trafficking to Cajal bodies and telomeres or is required for telomerase catalysis (Chen et al., 2018; Stern et al., 2012; Venteicher et al., 2009; Vogan et al., 2016; Zhong et al., 2011). In contrast, our results demonstrate that in the absence of TCAB1, TERT and TR are localized to the distinct sub-cellular compartments, the nucleoplasm and the nucleolus, respectively. This spatial separation prevents telomerase assembly, which leads to reduced number of telomerase RNPs per cell and in turn telomere shortening. Our conclusions are based on a variety of quantitative approaches analyzing telomerase assembly by purification of the telomerase RNP and in intact cells. Analysis of TERT localization in living and fixed cells clearly demonstrates that TERT is excluded from the nucleolus. Importantly, we confirmed that the nucleolar exclusion of TERT is not a consequence of the protein-tags used to visualize TERT in these experiments. Purification of telomerase from TCAB1 knock-out cells further confirmed that TCAB1 is required for telomerase assembly *in vivo*. The amount of TR and dyskerin associated with TERT is substantially reduced in the absence of TCAB1. Finally, we used live cell single-molecule imaging to demonstrate that the diffusion pattern of TERT molecules and their interactions with telomeres are significantly different in TCAB1 knock-out cells compared to control cells. More importantly, TERT movements in the absence of TCAB1 are comparable to those in TR knock-out cells where telomerase assembly is impossible. Altogether, these observations support our model that TCAB1 is required for telomerase assembly by extracting TR from the nucleolus to facilitate its assembly with TERT. Our model is further supported by work from Vogan et al., which demonstrated that truncated TR (hTRmin) that lacks the H/ACA region and therefore cannot bind dyskerin, accumulates in the nucleoplasm and is excluded from nucleoli (Vogan et al., 2016). Importantly, in cells that express hTRmin, TCAB1 is not essential for telomere maintenance (Vogan et al., 2016), consistent with TCAB1 promoting telomerase assembly by extracting TR from the nucleolus.

Previous work by others has reported conflicting results regarding the role of TCAB1 in telomerase catalysis, ranging from full enzymatic activity in initial reports to substantial activity defects in the most recent study (Chen et al., 2018; Venteicher et al., 2009; Vogan et al., 2016). Importantly, both our work and the only other study that analyzed the role of TCAB1 in telomerase activity using the "gold-standard" direct telomerase extension assay concluded that telomerase activity is reduced to approximately 20-30% in the absence of TCAB1. In both cases, telomerase was purified from TCAB1 knock-out cells using an antibody raised against TERT prior to measuring telomerase activity. While both studies concur on the degree to which telomerase activity is reduced in the absence of TCAB1, the proposed underlying molecular mechanisms differ. Chen et al. propose that TCAB1 is required for proper folding of the CR4/CR5 region of the telomerase RNA, which directly associates with TERT, without affecting telomerase assembly (Chen et al., 2018). Recent structural analysis of the telomerase RNP from human cells revealed that TCAB1 is located far away from the CR4/CR5 region of TR (Fig. S8)(Ghanim et al., 2021). TCAB1 resides within the H/ACA lobe of while CR4/CR5 is located within the catalytic lobe of the telomerase RNP. The two lobes are connected by the P1 and P4.2 helices which can adopt multiple conformations. Importantly, TCAB1 was not located near the CR4/CR5 region of TR in any of the observed telomerase RNP conformations (Ghanim et al., 2021). Although it is possible that telomerase can adopt additional conformations, based on the currently available structural information it is difficult to rationalize a molecular mechanism by which TCAB1 could specifically promote CR4/CR5 folding. In addition, due to the miss-folding of TR telomerase was proposed to adopt a low activity state in the absence of TCAB1. Experimentally such a low activity state would manifest itself as a reduction in the specific activity of telomerase (telomerase activity per assembled telomerase RNP). Our experiments strongly suggest that, while telomerase assembly is reduced in the absence of TCAB1, the limited amount of telomerase that can assemble is fully active (i.e. does not have reduced specific activity). Both, our enzymatic analysis and the positioning of TCAB1 within the telomerase RNP do not support a role of TCAB1 in TR folding and telomerase catalysis but are fully consistent with TCAB1 promoting telomerase assembly.

TCAB1 is necessary for the localization of scaRNAs to Cajal bodies and previous work suggested that it is also required for telomerase recruitment to telomeres (Stern et al., 2012; Venteicher et al., 2009). Our observations demonstrate that when TERT and TR are overexpressed in TCAB1 knock-out cells a fraction of TERT can assemble with TR an localize to telomeres. Telomerase recruitment to telomeres requires a direct interaction between TERT and TPP1 (Nandakumar et al., 2012; Schmidt et al., 2014; Zhong et al., 2012), therefore TR that localizes to telomeres must be assembled with TERT. These results are fully consistent with our model that the spatial separation of TR and TERT in the absence of TCAB1 prevents telomerase assembly. When TR is overexpressed the capacity of the nucleolus to sequester TR may be saturated and excess TR can assemble with TERT and localize to telomeres. Importantly, our observations also suggests that TCAB1 is not required for telomerase localization to telomeres.

In addition to the mechanistic insight into the role of TCAB1 in telomerase function, our results also demonstrate that nucleolar phase separation can effectively regulate telomerase RNP assembly in the nucleus of human cells. Binding of the H/ACA complex to the 3'-end of TR is essential for its stability (Mitchell et al., 1999), but also targets TR to the nucleolus preventing its assembly with TERT,

unless TCAB1 is present to extract TR from the nucleolus. Therefore, TCAB1 must have specific activities that counteract the propensity of the H/ACA complex to undergo liquid-liquid phase separation with components of the nucleolus. Our model also suggests that aberrant phase-separation of TR within the nucleolus underlies the telomerase deficiency observed in dyskeratosis congenita patients with TCAB1 mutations. Dissecting the molecular mechanism by which TCAB1 extracts TR from the nucleolus in future studies will undoubtably shed light on the fundamental principles of liquid-liquid phase separation and its physiological role in cell biology.

ACKNOWLEDGEMENTS
We would like to thank members of the Schmidt lab and J. Nandakumar for discussions and critical reading of the manuscript. This work was support by a grant from the NIH (R00 GM120386) to J.C.S. J.C.S. is a Damon Runyon Dale F. Frey Scientist supported (in part) by the Damon Runyon Cancer Research Foundation (DFS-24-17). S.B.C. acknowledges sustained support from the Ernest Piroska Major Foundation. This preprint was generated using a template from Ricardo Henriques.

AUTHOR CONTRIBUTIONS
B.S.A.-M. carried out IF-FISH experiments, telomerase purifications, analyzed telomerase assembly, generated mCherry- and 3xFLAG-HaloTag-dyskerin plasmids, determined their sub-cellular localization, and edited the manuscript. G.I.P. maintained cell lines, established TCAB1 and TR knockout cell lines and carried out IF-FISH experiments. K.A.-B. assisted in establishing the TR knockout cell line and carried out characterization of the TR knockout cells. S.B.C. purified and characterized the anti-TERT sheep antibody. L.H. and K.Y. characterized TCAB1 knock-out clones using Southern blots. J.C.S. carried out all other experiments, designed the research, analyzed data, and wrote the manuscript.

COMPETING INTERESTS
The authors declare no competing interests.

Methods

Cell Lines and Tissue Culture. All cell lines were based on HeLa-EM2-11ht (Weidenfeld et al., 2009) and were cultured in Dulbecco's Modified Eagle Medium including L-glutamine (Gibco) supplemented with 10% fetal bovine serum, 100 units/ml penicillin and 100 µg/ml streptomycin at 37°C with 5% CO_2. Live cell imaging was carried out using CO2 independent media supplemented with 2 mM GlutaMAX (Life Technologies), 10% fetal bovine serum, 100 units/ml penicillin and 100 µg/ml streptomycin at 37°C with 5% CO_2. For single-molecule imaging of HaloTag-TERT cell were cultured in homemade imaging dishes made by gluing 22x22 mm Nexterion coverslips (170 ± 5 µm, Schott) onto the bottom of plastic 3.5 x 1.0 cm cell culture dishes with a hole in the middle using an epoxy adhesive. Prior to chamber assembly the coverslips were washed with 1 M KOH and 100% for 30 min each in a sonicating water bath. To enrich for cells in S-phase for live cell imaging experiments, cultures we treated with complete media including 2 mM thymidine for a minimum of 16 hours. Cells were released 2 hours prior to imaging by replacing the thymidine containing media with fresh media without thymidine. Puromycin selection was carried out at a concentration of 1 µg/ml.

Plasmid Construction and Genome Editing. All plasmids were generated by Gibson assembly (NEB) using standard protocols or by inverse PCR. All plasmids will be made available on Addgene. All Cas9 and sgRNA expression plasmids were based on pX330 (Cong et al., 2013). The homologous recombination donor for the TR knockout was generated by assembling the genomic sequences immediately upstream and downstream (500 bp each) of the TR sequence flanking a puromycin resistance cassette into HpaI linearized pFastBac. The 3xFLAG-HaloTag-NLS plasmids was generated by adding a 3xFLAG-tag to a previously described HaloTag-NLS plasmid (a kind gift from X. Darzacq and A. Hansen) (Hansen et al., 2018). The 3xFLAG-HaloTag-dyskerin plasmid was generated by replacing TERT in our previously described 3xFLAG-HaloTag-TERT expression plasmid with the dyskerin coding sequence (Schmidt et al., 2016). The mCherry-dyskerin plasmid was generated by replacing TERT in our previously described mCherry-TERT expression plasmid with the dyskerin coding sequence (Schmidt et al., 2014). All transfections were carried out using Lipfectamine 2000 (Invitrogen) using the manufacturer's instructions. TCAB1 was knocked-out using two separate sgRNA plasmids that were transfected alongside a GFP-expression plasmid. 24 hours after transfection single-cell clones were sorted using the GFP signal. TCAB1 knock-out clones were screened by western blot and confirmed by Southern Blotting of the TCAB1 locus and immunofluorescence imaging. TR was knocked out by transfecting two sgRNA plasmids and a homologous recombination donor plasmid. 48 hours after transfection puromycin selection was initiated and 1 week after the initiation of selection single-cell clones were generated by dilution into 96-well plates. TR knock-out was confirmed using PCR and Sanger sequencing, fluorescence in situ hybridization, and RT-qPCR.

Immunofluorescence and Fluorescence In Situ Hybridization Imaging. Fixed cell immunofluorescence imaging and fluorescence in situ hybridization was carried out as previously described (Schmidt et al., 2014). Briefly, cells grown on coverslips were fixed in PBS supplemented with 4% formaldehyde. When using the HaloTag for fluorescence detection cells were incubated with 100 nM of JF646 HaloTag-ligand for 30 min prior to fixation. Unincorporated ligand was removed by 3 washes with complete media followed by placing the cells back in the incubator for 10 min to let additional dye leak out of the cells. mEOS3.2-TRF2 was detected using the intrinsic fluorescence of green form of mEOS3.2. After removing the fixation solution using 2 PBS washes, coverslips were transferred into aluminum foil covered humidity chambers with a parafilm layer and rinsed with 1 ml of PBS with 0.2% Triton X-100. Cells were than incubated in blocking buffer (PBS, 0.2% Triton X-100, 3% BSA) for 30 minutes, followed by incubation with primary antibodies diluted in blocking buffer for 1 hour. All primary antibodies (see key resource table) were used at a concentration of 1 µg/ml. After three washes with PBS + 0.2% Triton X-100, coverslips were incubated with secondary antibodies diluted in PBS + 0.2% Triton X-100 for 1 hour. All secondary antibodies (see key resource table) were used at a concentration of 4 µg/ml. Cells were washed three times PBS + 0.2% Triton X-100 prior to a second fixation with PBS + 4% formaldehyde. In cases were nuclear staining

was used the first of the three washing steps also included 0.1 µg/ml HOECHST. After the second fixation steps coverslips were dehydrates in three steps with ethanol (70%, 95%, 100%), re-hydrated in 2xSSC + 50% formamide, blocked for 1 hour in hybridization buffer (100 mg/ml dextran sulfate, 0.125 mg/ml E. coli tRNA, 1 mg/ml nuclease free BSA, 0.5 mg/ml salmon sperm DNA, 1 mM vanadyl ribonucleoside complexes, 50% formamide, 2xSSC) at 37°C, before incubating the coverslips in hybridization buffer supplemented with three TR probes (30 ng per coverslip) over night at 37°C. Probe sequences were previously described (Tomlinson et al., 2006). After hybridization coverslips were washes twice for 30 minutes in 2xSSC + 50% formamide and then mounted on slides using ProLong Antifade Diamond mounting media (Life Technologies). Microscopy was carried out using a DeltaVision Elite microscope using a 60x PlanApo objective (1.42 NA) and a pco.edge sCMOS camera. We acquired 20 Z-sections spaced by 0.2 µm, followed by image deconvolution and maximum intensity projection of the sections using the DeltaVision Softworx software. For the quantification of cellular TR distribution in control and TCAB1 knockout cells we assigned cells into one of three categories: Cells with TR only at telomeres, Cells with TR only in nucleoli, Cells with TR at telomeres and in nucleoli. We carried out 3 independent biological replicates and counted a minimum of 100 cells for control and TCAB1 knockout cells.

Single-Molecule Live Cell Imaging. Live cell single-molecule imaging was carried out on a Olympus IX83 inverted microscope equipped with a 4-line cellTIRF illuminator (405 nm, 488 nm, 561 nm, 640 nm lasers), a Olympus UAPO 100x TIRF objective (1.49 NA), a CAIRN TwinCam beamsplitter, 2 Andor iXon 897 Ultra EMCCD cameras, and a blacked-out environmental control enclosure. The microscope was operated using the Olympus cellSense software. 3xFLAG-HaloTag-TERT was labeled for 2 min in complete media supplemented with 100 nM JF646-HaloTag ligand (Grimm et al., 2015). After removing the HaloTag-ligand with three washes in complete media, cells were placed back in the incubator for 10 min to allow unincorporated dye to leak out of the cells. Cells were then transferred into CO2 independent media and put on the microscope which was heated to 37°C. Single-molecule imaging was carried out at 100 frames per second using highly inclined laminated optical sheet illumination (Tokunaga et al., 2008). Movies were typically 20 seconds in length (2000 frames) and were followed by a transmitted light acquisition to visualize overall cell morphology.

RT-qPCR. RNA samples for RT-qPCR analysis were generated by using RNA mini prep kits (Zymogen) using 2 million cells as starting material. Reverse transcription was carried out using random hexamer primers and SuperScript III reverse transcriptase (Invitrogen) according to the manufacturer's instructions. qPCR was carried out using the Maxima SYBR Green qPCR master mix (Thermo Scientific) using primers for GAPDH and TR according to the manufacturer's instructions. All qPCR reactions were carried out in triplicates and three independent biological replicates were analyzed. RT-qPCR experiments were carried out in triplicate and the TR Ct value was normalized to the GAPDG Ct value.

Southern Blotting. Southern blotting was carried out using standard protocols (Southern, 2006). Briefly, genomic DNA generated by phenol-chloroform extraction after cell lysis using TE supplemented with 0.5% SDS and 0.1 mg/ml Proteinase K, was digested with BamHI (generating a 1394 bp fragment spanning exons 1-3 of the TCAB1 locus) and separated on a 0.8% agarose gel. The DNA was then transferred on a Hybond-N+ nylon membrane using capillary transfer. The TCAB1 locus was detected using radioactive probes (alpha-^{32}P-dCTP) generated by randomly primed DNA synthesis using an 800 bp PCR product from within the 1394 bp restriction fragment as a template and Klenow polymerase (NEB).

Western Blotting. Mini-PROTEAN TGX stain-free gels (Bio-Rad) were used for SDS-PAGE. Total protein was detected using a ChemiDoc MP (Bio-Rad) after a 45 second UV activation. Western transfer was carried out using the Trans-Blot Turbo transfer system (Bio-Rad) according to the manufacturer's instructions using the mixed molecular weight transfer setting. Immuno-blotting was carried out using standard protocols. The TCAB1 antibody (Proteintech) was used at a 1:2000 dilution, the TERT antibody (Abcam) was used at a 1:4000 dilution, and the dyskerin antibody (Santa Cruz Biotech) was used at a 1:200 dilution. Secondary antibodies were used at a 1:10000 dilution.

Northern Blotting. RNA was extracted from cell lysates and purified telomerase samples supplemented with 10 ng of a loading and recovery control (*in vitro* transcribed TR 34-328) using the RNeasy Mini kit (Qiagen) and eluted in 30 ul of RNase free water. 15 ul of eluted RNA was mixed with 15 ul of 2x formamide loading buffer (0.1XTBE, 25 mM EDTA, 0.1% bromophenol blue, 0.1% xylene cyanol, 93% formamide) and heated to 60°C for 5 min. Samples were separated on a 6% TBE, 7M Urea, polyacrylamide gel (Life Technologies), and transferred to a Hybond N+ membrane (Cytiva) using a wet-blotting apparatus in 1x TBE for 2 hours at 0.5 A of constant current in the cold room. After transfer, membranes were UV-crosslinked, and pre-hybridized in Church buffer for 2 hours at 50°C. Three DNA oligos complementary to TR were radioactively labeled using T4 PNK (NEB) and $10x10^6$ cpm of each probe were added to the membrane. Hybridization was carried out at 50°C overnight. Membranes were washed three times with 2xSSC, 0.1% SDS prior to exposure to a storage phosphorescence screen (Cytiva) which was then imaged on an Amersham Typhoon IP phosphoimager (Cytiva).

Telomerase Expression and Purification. Cell lines were transfected in 15 cm tissue culture plates at 90% confluency ($25\text{-}30x10^6$ cells) using 7.5 µg of TERT plasmid, 30 µg of TR plasmid and 75 µl of Lipofectamine 2000 in 1875 ul of

Opti-MEM (Cristofari and Lingner, 2006). Transfected cells were split to three 15 cm dishes 24 hours after transfection. 48 hours after transfection cells were counted, harvested, and snap frozen in liquid nitrogen. Cells were lysed in 1 ml of CHAPS lysis buffer supplemented with 5 µl of RiboLock RNase inhibitor (10 mM TRIS pH 7.5, 1 mM $MgCl_2$, 1 mM EGTA pH 8.0, 0.5% CHAPS, 10% glycerol) per $100x10^6$ cells and rotated at 4°C for 30 min. Lysates were cleared in a table-top centrifuge at 21,000xg for 15 min at 4°C. Identical cell equivalents were used for all samples. 45 µg of anti-TERT antibody was added per ml of cleared lysate and samples were rotated for 1 hour at 4°C. Lysates were then added to 100 µl of protein G agarose and rotated for 1 hour at 4°C. The resin was spun down at 1000xg and washed four times with 1 ml of Buffer W (20 mM HEPES pH 7.9, 300 mM KCl, 2 mM $MgCl_2$, 1 mM EDTA, 1 mM DTT, 1 mM PMSF, 0.1% Triton X-100, 10% glycerol). TERT was eluted in 100 µl of Buffer W supplemented with 5 µl of 1 mM TERT peptide by rotating for 30 min at room temperature.

Telomerase Activity Assays. Telomerase assays were carried out in 20 µl of reaction buffer (50 mM TRIS pH 8.0, 150 mM KCl, 1 mM $MgCl_2$, 2 mM DTT, 100 nM TTAGGGTTAGGGTTAGGG oligo, 10 µM dATP, 10 µM dGTP, 10 µM dTTP, 0.165 µM dGTP [α-32P] 3000 Ci/mmol) including 2 µl of purified telomerase for 1 hour at 30°C. Telomerase was incubated with the substrate oligo for 15 min at room temperature, prior to initiating the reaction by addition of dNTPs. Reactions were stopped by adding 100 µl of 3.6 M ammonium acetate supplemented with 20 µg of glycogen and 32P 5'-end labeled loading control oligos (TTAGGGTTAGGGTTAGGG, TTAGGGTTAGGGTTAG). Reaction products were precipitated using 500 µl of ice-cold ethanol and stored at -20°C over-night. Reaction products were spun down in a table-top centrifuge at max speed for 30 min at 4°C, washed with 500 µl of 70% ethanol, and spun down again speed for 30 min at 4°C. The 70% ethanol was decanted, and the reaction products were dried in an Eppendorf vacuum concentrator at 45°C. Reaction products were resuspended in 20 µl of loading buffer (0.05XTBE, 25 mM EDTA, 0.05% bromophenol blue, 0.05% xylene cyanol, 46.5% formamide) and incubated at 95°C for 5 min. 10 µl of each sample was separated on a 12% polyacrylamide, 7 M urea sequencing gel pre-run for 45 min at 90W. Gels were dried and exposed to a storage phosphorescence screen (Cytiva) and imaged on an Amersham Typhoon IP phosphoimager (Cytiva).

Single-Particle Tracking. Single-particle tracking was carried out in MATLAB 2019a using a batch parallel-processing version of SLIMfast modified to allow the input of TIFF files (kindly provided by Xavier Darzacq and Anders Hansen) (Hansen et al., 2018), an implementation of the Multiple-Target-Tracing algorithm (Sergé et al., 2008), with the following settings: Exposure Time = 10 ms, NA = 1.49, Pixel Size = 0.16 µm, Emission Wavelength = 664 nm, Dmax = 5 $\mu m^2/s$, Number of gaps allowed = 2, Localization Error = 10^{-5}, Deflation Loops = 0. Diffusion coefficients and the fraction of molecules in each distinct particle population were determined using the MATLAB version of the SpotOn tool (kindly provided by Xavier Darzacq and Anders Hansen) (Hansen et al., 2018) with the following settings: TimeGap = 10 ms, dZ = 0.700 µm, GapsAllowed = 2, TimePoints = 8, JumpsToConsider = 4, BinWidth = 0.01 µm, PDFfitting, D_Free1_3State = [1 25], D_Free2_3State = [0.1 1], D_Bound_3State = [0.0001 0.1]. For all experiments we carried out 3 independent biological replicates with at least 15 cells for each cell line. The complete data set can be found in supplemental figure S6D. The statistical significance of differences in particle fractions and diffusion coefficients were assessed using a two-tailed T-Test.

Quantification of Fixed Cell Imaging. For the quantification of cellular TR distribution in control and TCAB1 knockout cells we assigned cells into one of three categories: Cells with TR only at telomeres, Cells with TR only in nucleoli, Cells with TR at telomeres and in nucleoli. We carried out 3 independent biological replicates and counted a minimum of 100 cells for control and TCAB1 knockout cells.

Quantification of RT-qPCR. RT-qPCR experiments were carried out in triplicate and the TR Ct value was normalized to the GAPDG Ct value. The meanCt (Ct of TR – Ct of GAPDH) value from three independent experiments and the corresponding standard deviation is shown in figure S6B.

Quantification of Western Blots, Northern Blots, and Telomerase Activity Assays. Gel images from Western Blots, Northern Blots, and Telomerase Activity Assays were analyzed using ImageQuant TL 8.2. To quantify TR levels in Northern blots the TR band intensity was normalized to the loading and recovery control signal added to the RNA sample prior to RNA purification. To quantify telomerase activity the whole lane intensity starting at repeat 1 was determined and divided by the sum of the loading control signals. Telomerase processivity was calculated by dividing product intensity > 7 repeats by the total signal in the respective lane. The statistical significance of the observed differences was calculated using a two-tailed T-test using a minimum of three biological replicates. Each biological replicate (independent telomerase expression and purification) was analyzed in technical triplicate.

References

Angrisani, A., Vicidomini, R., Turano, M., and Furia, M. (2014). Human dyskerin: beyond telomeres. Biol Chem 395, 593–610.

Armanios, M., and Blackburn, E.H. (2012). The telomere syndromes. Nat Rev Genet 13, 693-704.

Chen, L., Roake, C.M., Freund, A., Batista, P.J., Tian, S., Yin, Y.A., Gajera, C.R., Lin, S., Lee, B., Pech, M.F., et al. (2018). An Activity Switch in Human Telomerase Based on RNA Conformation and Shaped by TCAB1. Cell 174.

Cohen, S.B., Graham, M.E., Lovrecz, G.O., Bache, N., Robinson, P.J., and Reddel, R.R. (2007). Protein Composition of Catalyti-

cally Active Human Telomerase from Immortal Cells. Science 315, 1850–1853.

Cong, L., Ran, F.A., Cox, D., Lin, S., Barretto, R., Habib, N., Hsu, P.D., Wu, X., Jiang, W., Marraffini, L.A., et al. (2013). Multiplex Genome Engineering Using CRISPR/Cas Systems. Science 339, 819–823.

Cristofari, G., and Lingner, J. (2006). Telomere length homeostasis requires that telomerase levels are limiting. Embo J 25, 565-574.

Freund, A., Zhong, F.L., Venteicher, A.S., Meng, Z., Veenstra, T.D., Frydman, J., and Artandi, S.E. (2014). Proteostatic Control of Telomerase Function through TRiC-Mediated Folding of TCAB1. Cell 159, 1389-1403.

Ghanim, G.E., Fountain, A.J., Roon, A.-M.M. van, Rangan, R., Das, R., Collins, K., and Nguyen, T.H.D. (2021). Structure of human telomerase holoenzyme with bound telomeric DNA. Nature 1–5.

Grimm, J.B., English, B.P., Chen, J., Slaughter, J.P., Zhang, Z., Revyakin, A., Patel, R., Macklin, J.J., Normanno, D., Singer, R.H., et al. (2015). A general method to improve fluorophores for live-cell and single-molecule microscopy. Nat Methods 12, 244-50.

Hansen, A.S., Woringer, M., Grimm, J.B., Lavis, L.D., Tjian, R., and Darzacq, X. (2018). Robust model-based analysis of single-particle tracking experiments with Spot-On. Elife 7.

Harley, C.B., Futcher, A.B., and Greider, C.W. (1990). Telomeres shorten during ageing of human fibroblasts. Nature 345, 458-460.

Hyman, A.A., Weber, C.A., and Jülicher, F. (2014). Liquid-Liquid Phase Separation in Biology. Annu Rev Cell Dev Bi 30, 39–58.

Jády, B.E., Bertrand, E., and Kiss, T. (2004). Human telomerase RNA and box H/ACA scaRNAs share a common Cajal body–specific localization signal. J Cell Biology 164, 647–652.

Mitchell, J.R., Wood, E., and Collins, K. (1999). A telomerase component is defective in the human disease dyskeratosis congenita. Nature 402, 551-555.

Mitrea, D.M., and Kriwacki, R.W. (2016). Phase separation in biology; functional organization of a higher order. Cell Commun Signal Ccs 14, 1.

Nagpal, N., Wang, J., Zeng, J., Lo, E., Moon, D.H., Luk, K., Braun, R.O., Burroughs, L.M., Keel, S.B., Reilly, C., et al. (2020). Small-Molecule PAPD5 Inhibitors Restore Telomerase Activity in Patient Stem Cells. Cell Stem Cell 26, 896-909.e8.

Nandakumar, J., and Cech, T.R. (2013). Finding the end: recruitment of telomerase to telomeres. Nat Rev Mol Cell Bio 14.

Nandakumar, J., Bell, C.F., Weidenfeld, I., Zaug, A.J., Leinwand, L.A., and Cech, T.R. (2012). The TEL patch of telomere protein TPP1 mediates telomerase recruitment and processivity. Nature 492, 285-289.

Schmidt, J.C., and Cech, T.R. (2015). Human telomerase: biogenesis, trafficking, recruitment, and activation. Gene Dev 29, 1095-1105.

Schmidt, J.C., Dalby, A.B., and Cech, T.R. (2014). Identification of human TERT elements necessary for telomerase recruitment to telomeres. Elife 3, e03563.

Schmidt, J.C., Zaug, A.J., and Cech, T.R. (2016). Live Cell Imaging Reveals the Dynamics of Telomerase Recruitment to Telomeres. Cell 166, 1188-1197.e9.

Schmidt, J.C., Zaug, A.J., Kufer, R., and Cech, T.R. (2018). Dynamics of human telomerase recruitment depend on template-telomere base pairing. Mol Biol Cell 29, 869-880.

Sergé, A., Bertaux, N., Rigneault, H., and Marguet, D. (2008). Dynamic multiple-target tracing to probe spatiotemporal cartography of cell membranes. Nat Methods 5, 687-694.

Shukla, S., Schmidt, J.C., Goldfarb, K.C., Cech, T.R., and Parker, R. (2016). Inhibition of telomerase RNA decay rescues telomerase deficiency caused by dyskerin or PARN defects. Nat Struct Mol Biol 23, 286-292.

Shukla, S., Jeong, H.-C., Sturgeon, C.M., Parker, R., and Batista, L.F.Z. (2020). Chemical inhibition of PAPD5/7 rescues telomerase function and hematopoiesis in dyskeratosis congenita. Blood Adv 4, 2717–2722.

Southern, E. (2006). Southern blotting. Nat Protoc 1, 518–525.

Stern, J.L., Zyner, K.G., Pickett, H.A., Cohen, S.B., and Bryan, T.M. (2012). Telomerase Recruitment Requires both TCAB1 and Cajal Bodies Independently. Mol Cell Biol 32, 2384–2395.

Stewart, S.A., and Weinberg, R.A. (2006). Telomeres: Cancer to Human Aging. Annu Rev Cell Dev Bi 22, 531–557.

Stuart, B.D., Choi, J., Zaidi, S., Xing, C., Holohan, B., Chen, R., Choi, M., Dharwadkar, P., Torres, F., Girod, C.E., et al. (2015). Exome sequencing links mutations in PARN and RTEL1 with familial pulmonary fibrosis and telomere shortening. Nat Genet 47, 512-517.

Tokunaga, M., Imamoto, N., and Sakata-Sogawa, K. (2008). Highly inclined thin illumination enables clear single-molecule imaging in cells. Nat Methods 5, 159-161.

Tomlinson, R.L., Ziegler, T.D., Supakorndej, T., Terns, R.M., and Terns, M.P. (2006). Cell cycle-regulated trafficking of human telomerase to telomeres. Mol Biol Cell 17, 955-965.

Tseng, C.-K., Wang, H.-F., Burns, A.M., Schroeder, M.R., Gaspari, M., and Baumann, P. (2015). Human Telomerase RNA Processing and Quality Control. Cell Reports 13, 2232–2243.

Tummala, H., Walne, A., Collopy, L., Cardoso, S., Fuente, J. de la, Lawson, S., Powell, J., Cooper, N., Foster, A., Mohammed, S., et al. (2015). Poly(A)-specific ribonuclease deficiency impacts telomere biology and causes dyskeratosis congenita. J Clin Invest 125, 2151–2160.

Venteicher, A.S., Abreu, E.B., Meng, Z., McCann, K.E., Terns, R.M., Veenstra, T.D., Terns, M.P., and Artandi, S.E. (2009). A human telomerase holoenzyme protein required for Cajal body localization and telomere synthesis. Science 323, 644-648.

Vogan, J.M., Zhang, X., Youmans, D.T., Regalado, S.G., Johnson, J.Z., Hockemeyer, D., and Collins, K. (2016). Minimized human telomerase maintains telomeres and resolves endogenous roles of H/ACA proteins, TCAB1, and Cajal bodies. Elife 5, 693.

Weidenfeld, I., Gossen, M., Löw, R., Kentner, D., Berger, S., Görlich, D., Bartsch, D., Bujard, H., and Schönig, K. (2009). Inducible expression of coding and inhibitory RNAs from retargetable genomic loci. Nucleic Acids Res 37, e50.

Wu, R.A., Upton, H.E., Vogan, J.M., and Collins, K. (2017). Telomerase Mechanism of Telomere Synthesis. Annu Rev Biochem 86, 439-460.

Xi, L., and Cech, T.R. (2014). Inventory of telomerase components

in human cells reveals multiple subpopulations of hTR and hTERT. Nucleic Acids Res 42, 8565–8577.

Zhong, F., Savage, S.A., Shkreli, M., Giri, N., Jessop, L., Myers, T., Chen, R., Alter, B.P., and Artandi, S.E. (2011). Disruption of telomerase trafficking by TCAB1 mutation causes dyskeratosis congenita. Gene Dev 25, 11–16.

Zhong, F.L., Batista, L.F.Z., Freund, A., Pech, M.F., Venteicher, A.S., and Artandi, S.E. (2012). TPP1 OB-Fold Domain Controls Telomere Maintenance by Recruiting Telomerase to Chromosome Ends. Cell 150, 481-494.

Supplementary Movie Legends

Movie S1. Single-particle tracking of 3xFLAG-HaloTag-TERT labeled with JF646 in a control cell acquired at 100 frames per second. Trajectories with a minimum of 5 localizations are displayed. 150x150 pixels with a pixel size of 0.16 μm.

Movie S2. Single-particle tracking of 3xFLAG-HaloTag-TERT labeled with JF646 in a TCAB1 knockout cell acquired at 100 frames per second. Trajectories with a minimum of 5 localizations are displayed. 150x150 pixels with a pixel size of 0.16 μm.

Movie S3. Movie of cell expressing GFP-nucleolin (red) and 3xFLAG-HaloTag-NLS (green) labeled with JF646 acquired at 100 frames per second, showing overlap of 3xFLAG-HaloTag-NLS with nucleoli. 140x140 pixels with a pixel size of 0.16 μm.

Movie S4. Movie of 3xFLAG-HaloTag-TERT labeled with JF646 in a control (left), TCAB1 knockout (middle), and TR knockout (right) cell acquired at 100 frames per second. Each panel is 150x150 pixels in size with a pixel size of 0.16 μm.

Movie S5. Single-particle tracking of 3xFLAG-HaloTag-TERT labeled with JF646 in a TR knockout cells acquired at 100 frames per second. Trajectories with a minimum of 5 localizations are displayed. 150x150 pixels with a pixel size of 0.16 μm.

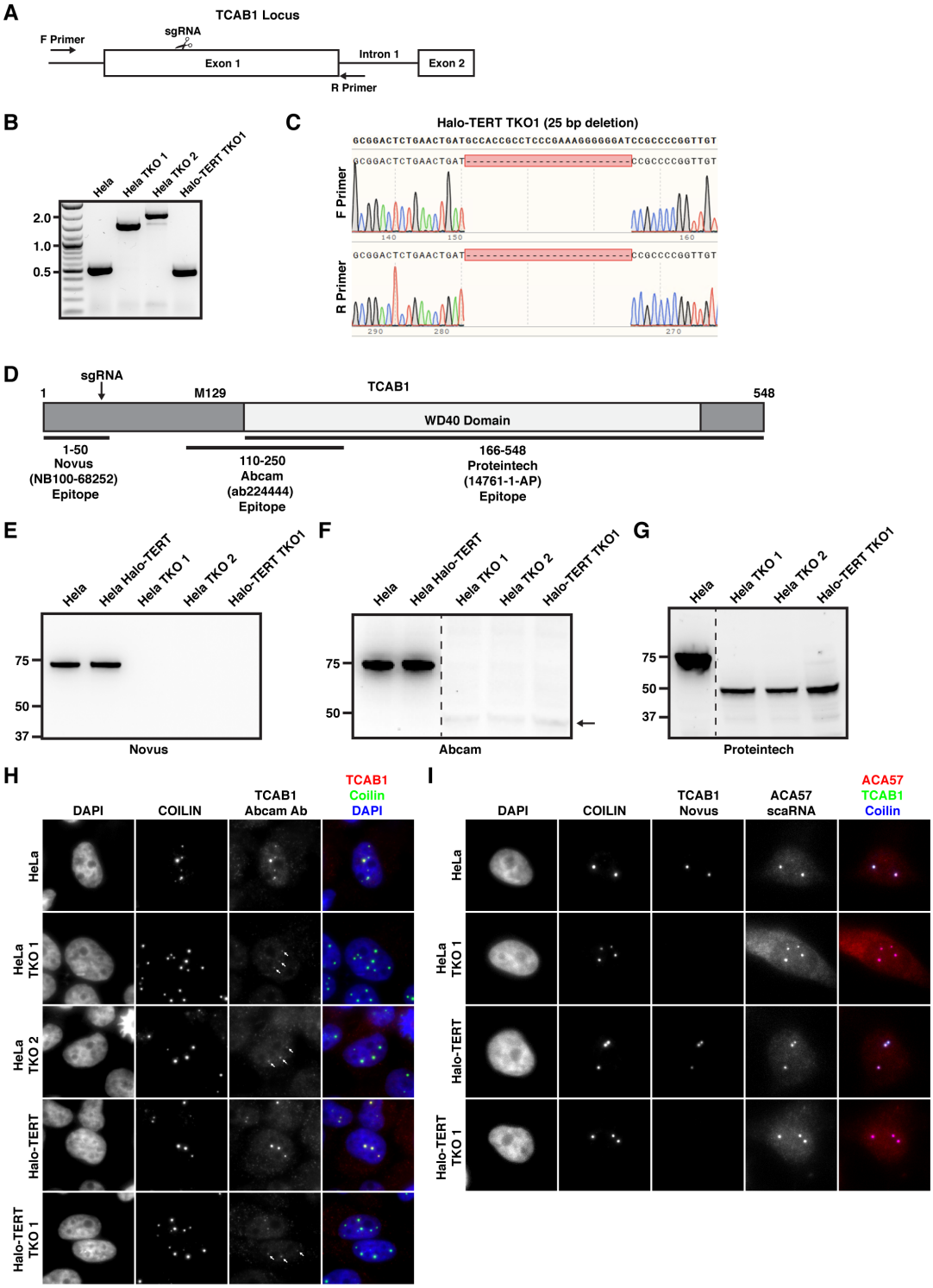

Supplementary Figure 1. **A** Strategy to knock-out TCAB1 with a single Cas9 and a single sgRNA targeting exon 1 of the TCAB1 gene. **B** PCR of TCAB1 knock-out clones using the primers indicated in **A** demonstrating the absence of a WT TCAB1 allele. **C** Sanger sequencing of the PCR product derived from Halo-TERT TKO1 (B) demonstrating deletion causing a frame shift. (D) Model of TCAB1 protein indicating the antigens used to raise the indicated TCAB1 antibodies. **E-G** Western blots of parental cells and TCAB1 knock-out clones using **E** the Novus Biological, **F** Abcam, and **G** Proteintech TCAB1 antibodies, demonstrating the presence of a truncated TCAB1 protein in the putative TCAB1 knock-out cells. **H** IF using antibodies against coilin and TCAB1 (Abcam) demonstrating that truncated TCAB1 can be detected in Cajal bodies (white arrows) in putative TCAB1 knock-out clones. **I** IF using coilin and TCAB1 (Novus Biologicals) antibodies coupled to FISH with probes against the scaRNA ACA57, demonstrating that the Novus Biologicals antibody fails to detect the truncated TCAB1 and scaRNA localization is unchanged in putative TCAB1 knock-out cells.

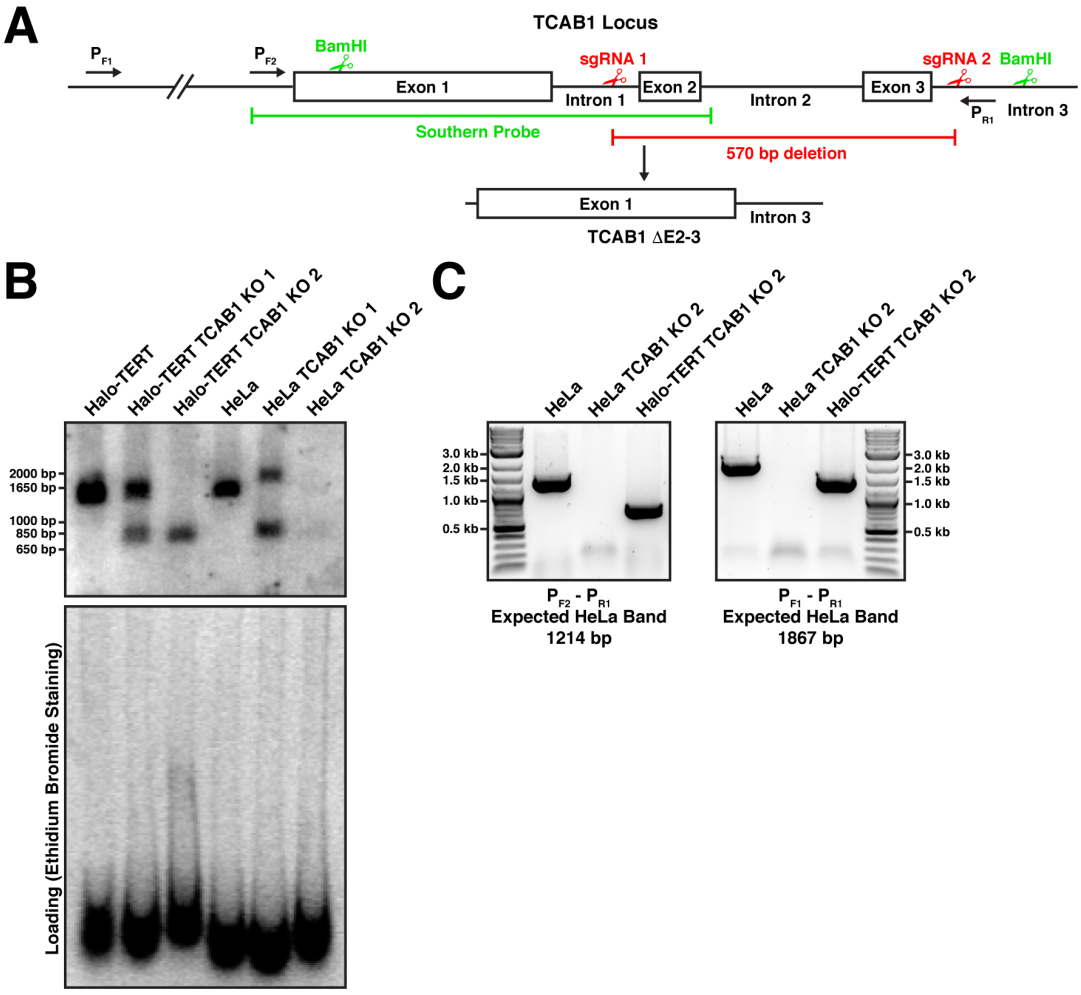

Supplementary Figure 2. **A** Strategy to knock-out TCAB1 using Cas9 and two sgRNAs targeting introns 1 and 3. **B** Southern blot of genomic DNA digested with BamHI from parental cells and TCAB1 knock-out clones using a probes generated from a PCR product of the TCAB1 gene indicated in **A** demonstrating the expected truncation of the TCAB1 gene in Halo-TERT TCAB1 KO 2. HeLa TCAB1 KO 2 carries larger deletions completely removing exons 1 and 2 from the TCAB1 gene. **C** PCR using primers indicated in **A** of genomic DNA from parental cells and TCAB1 knock-out clones confirming the deletion of critical regions of the TCAB1 gene show in **B**.

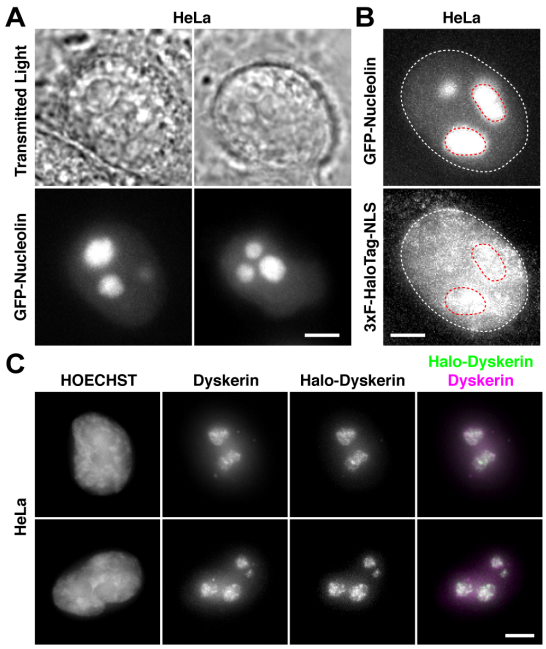

Supplementary Figure 3. **A** Images of HeLa cells transiently expressing GFP-nucleolin to mark nucleoli. The GFP-nucleolin signal overlaps with circular shapes visible under transmitted light illumination (scale bar = 2 µm). **B** Images of HeLa cells transiently expressing GFP-nucleolin and 3xFLAG-HaloTag-NLS labeled with JF646. The 3xFLAG-HaloTag-NLS signal (maximum intensity projection of 1000 frames of a single-molecule imaging movie) clearly overlaps with the GFP-nucleolin signal (red dashed outline), demonstrating that 3xFLAG-HaloTag-NLS can enter the nucleolus (scale bar = 2 µm). **C** Images of HeLa cells transiently expressing 3xFLAG-HaloTag-dyskerin labeled with JF646 and probed with an antibody against dyskerin, demonstrating that 3xFLAG-HaloTag-dyskerin localizes to the nucleolus (scale bar = 5 µm).

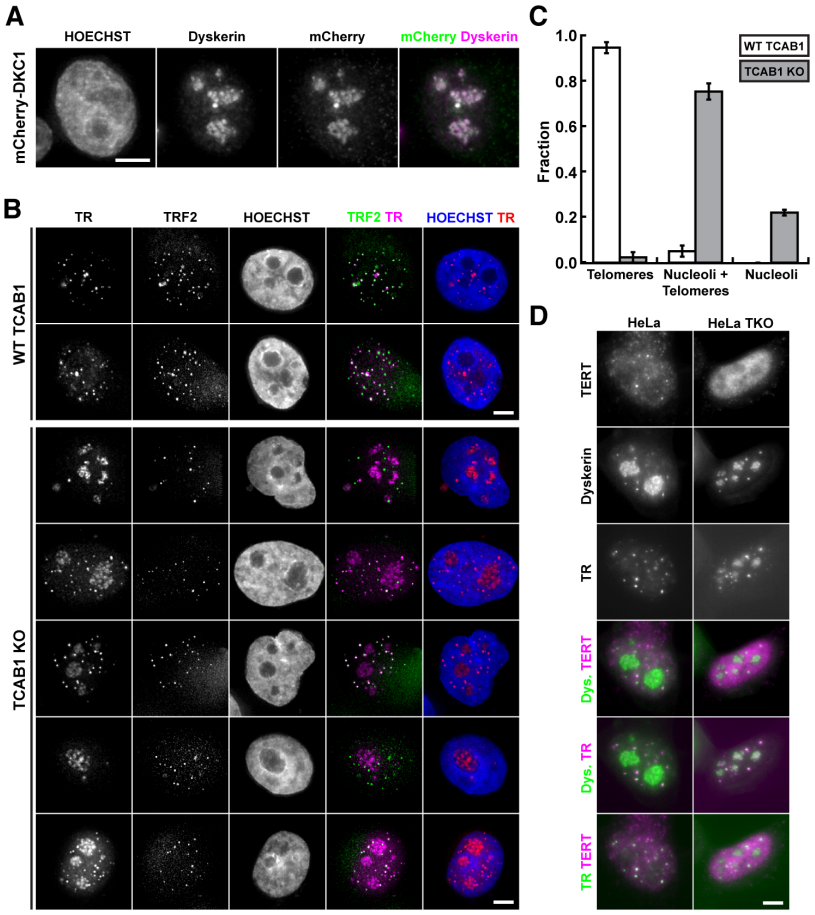

Supplementary Figure 4. A Images of HeLa cells transiently expressing mCherry-dyskerin probed with antibodies agains mCherry and dyskerin, demonstrating that mCherry dyskerin localizes to the nucleolus (scale bar = 5 µm). **B** Images of control and TCAB1 knock-out HeLa cells (3xFLAG-Halo-TERT, mEOS3.2-TRF2) overexpressing untagged TERT and TR. TR was detected using FISH and TRF2 was visualized using the fluorescence signal from mEOS3.2-TRF2. In control cells TR co-localizes with telomeres, while it is enriched in nucleoli and localized to telomeres in TCAB1 KO cells (scale bar = 5 µm). **C** Quantification of the fraction of cells showing TR localization exclusively to telomeres, to telomeres and nucleoli, or only to nucleoli (2 independent experiments, >100 cells per experiments, mean ± standard deviation). **D** Images of HeLa cells and TCAB1 knockout cells transiently expressing untagged TERT and TR probed with TERT (Abcam) and dyskerin antibodies and FISH for TR demonstrating that untagged TERT is excluded from nucleoli marked by dyskerin in parental and TCAB1 knock-out cells.

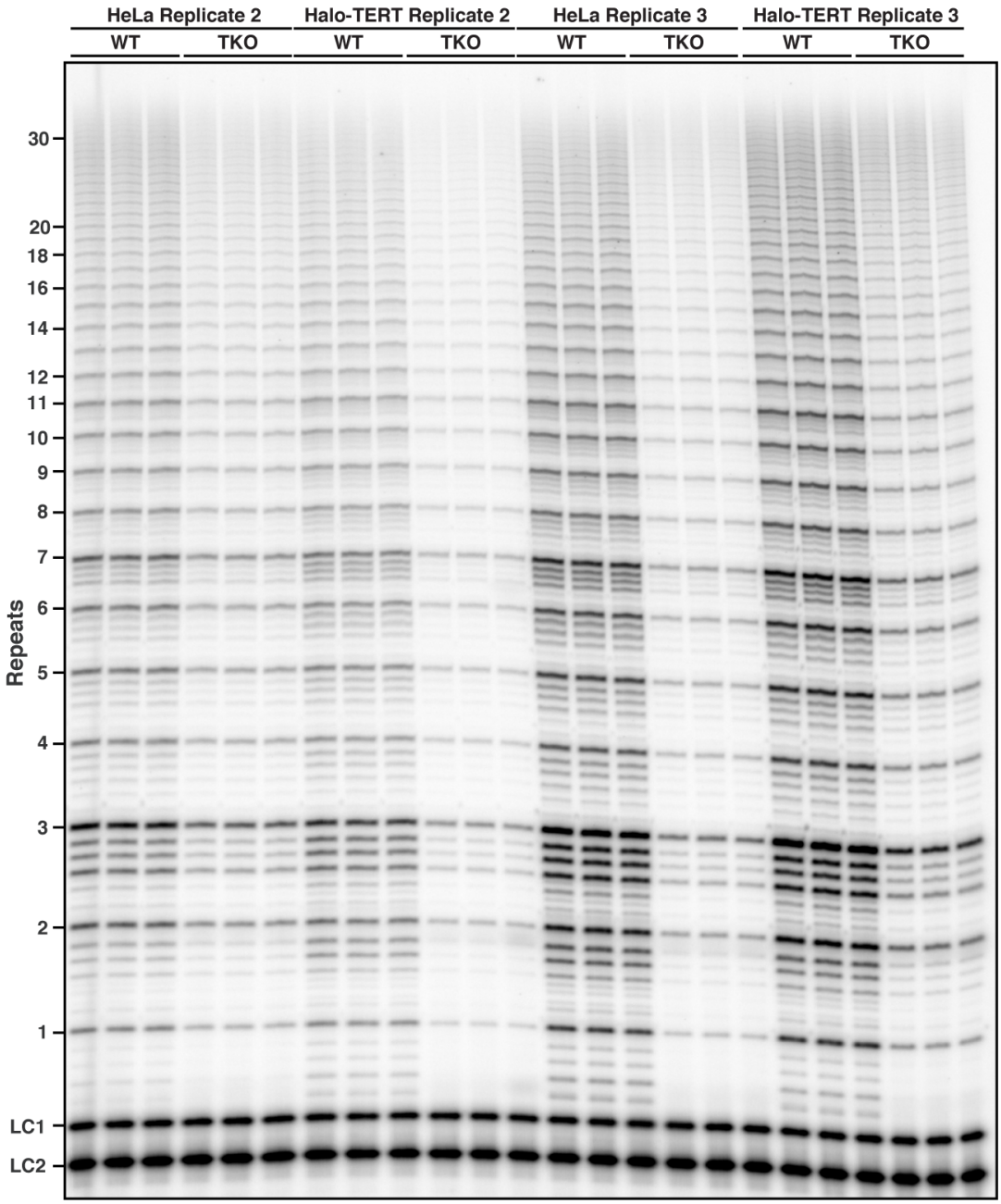

Supplementary Figure 5., Direct telomerase extension assay of telomerase immuno-purified from parental (WT) and TCAB1 knock-out (TKO) HeLa and Halo-TERT cell lines. LC1 and LC2, radiolabeled DNA oligonucleotide loading controls.

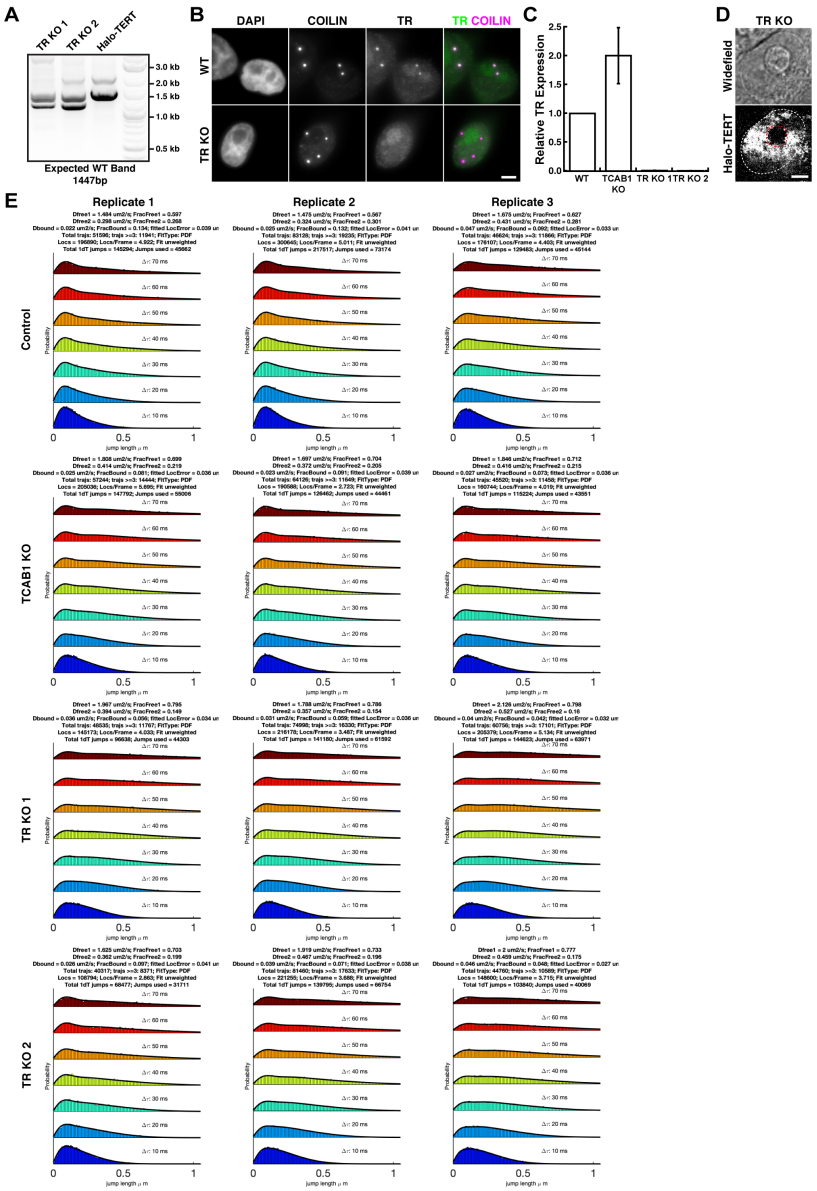

Supplementary Figure 6. **A** PCR analysis of the TR locus in parental and TR knock-out clones. Both TR knock-out clones show PCR products with reduced length that were confirmed to be knock-outs by Sanger sequencing. **B** Images of control and TR knock-out cells probed with an antibody against coilin and FISH probes specific for TR, demonstrating the lack of TR signal in TR knock-out cells (scale bar = 5 μm). **C** Determination of TR levels in control, TCAB1 knock-out, and TR knock-out cells, using RT-qPCR with primers specific to TR normalized to GAPDH (3 independent biological replicates, 3 technical replicates for each biological replicate, mean ± standard deviation). **D** Maximum intensity projection of 2000 frames of a 3xFLAG-HaloTag (JF646) TERT movie (bottom), demonstrating that the TERT signal does not overlap with the nucleolus detected as circular shape in the transmitted light image (top, red dashed line). **E** Fitting of single-particle tracking data of TERT from control, TCAB1 knock-out, and TR knock-out cells expressing 3xFLAG-HaloTag-TERT using the Spot-On tool.

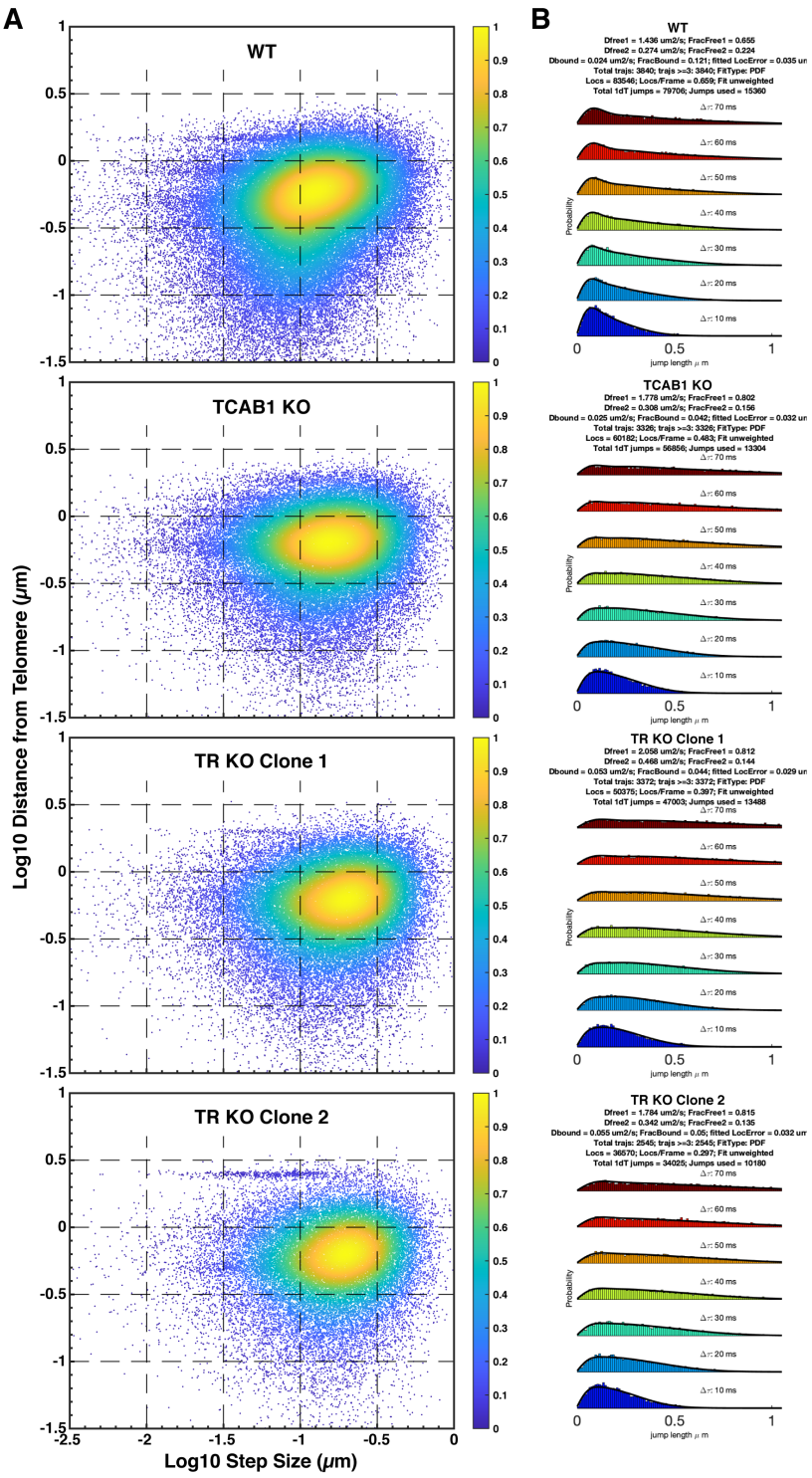

Supplementary Figure 7. **A** Analysis if the step size of telomeric TERT particles relative to the distance of the particle to the closest telomere (pooled results from 3 independent biological replicates with 19-30 cells analyzed per replicate). TERT molecules bound to the telomere are expected to have small step sizes and a short distance to the closest telomere, which is apparent in the enrichment of events in the lower quadrants in the WT control. This enrichment is not observed in TCAB1 and TR knock-out cells. **B** Spot-On analysis of telomeric TERT particles (pooled results from 3 independent biological replicates with 19-30 cells analyzed per replicate). The fraction of bound TERT particles in TCAB1 and TR knock-out cells is 4-5%, compared to 12% in the WT control cells.

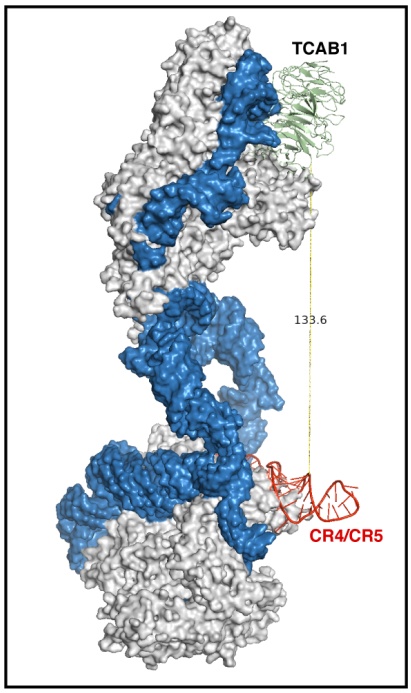

Supplementary Figure 8. Structure of the telomerase RNP showing the distance between TCAB1 and CR4/CR5 (13.4 nm). TR in blue, CR4/CR5 in red and TCAB1 in green.

REAGENTS AND RESOURCES

REAGENT or RESOURCE	SOURCE	IDENTIFIER
Antibodies		
anti-TCAB1 rabbit polyclonal antibody	Proteintech	14761-1-AP
anti-TCAB1 rabbit polyclonal antibody	Abcam	ab224444
anti-TCAB1 rabbit polyclonal antibody	Novus Biologicals	NB100-68252
anti-Coilin mouse monoclonal antibody	Abcam	ab87913
anti-Dyskerin mouse monoclonal antibody	Santa Cruz Biotech.	sc-373956
anti-TERT recombinant rabbit monoclonal antibody	Abcam	ab30202
anti-TERT sheep polyclonal antibody	Scott Cohen	Abx120550
anti-Rabbit Cy3 secondary antibody	Invitrogen	A-10520
anti-Mouse Alexa 647 secondary antibody	Invitrogen	A-21235
anti-Mouse Alexa 405 secondary antibody	Invitrogen	A-31553
anti-Mouse HRP	Invitrogen	A-31430
anti-Rabbit HRP	Invitrogen	A-31460
Chemicals, Peptides, and Recombinant Proteins		
JF646 HaloTag Ligand	Grimm et al., 2015	N/A
Prolong Diamond Antifade Mountant	Life Technologies	P36970
Thymidine	Sigma	T1895
Puromycin 10 mg/ml	Gibco	A1113803
Lipofectamine 2000	Invitrogen	11668019
dGTP [α-32P] 3000 Ci/mmol 10 mCi/ml	Perkin Elmer	BLU514H250UC
TERT peptide ARPAEEATSLEGALSGTRH	Cohen et al. 2008	N/A
Dextrane sulfate	Sigma	D8906-10G
E. coli tRNA	Sigma	10109541001
Salmon Sperm DNA	Invitrogen	15632011
Vanadyl Ribonucleoside Complexes	Sigma	R3380-5ML
Clarity Western ECL substrate	Bio-Rad	1705061
Experimental Models: Cell Lines		
HeLa EM2-11ht, TCAB1 KO	This paper	N/A
HeLa EM2-11ht, FLAG-HaloTag-TERT WT, HA-mEOS3.2-TRF2	Schmidt et al. 2016	N/A
HeLa EM2-11ht, FLAG-HaloTag-TERT WT, HA-mEOS3.2-TRF2, TCAB1 KO	This paper	N/A
HeLa EM2-11ht, FLAG-HaloTag-TERT WT, HA-mEOS3.2-TRF2, TR KO	This paper	N/A
Oligonucleotides		
TCAB1 sgRNA1 aaacctgggtcgccaagcaa	This paper	N/A
TCAB1 sgRNA2 ctgcacatttaagtccttcg	This paper	N/A
TCAB1 sgRNA for single cut knock-out GCCACCGCCTCCCGAAAGGG	This paper	N/A
TR sgRNA1 ACCCTAACTGAGAAGGGCGT	This paper	N/A
TR sgRNA2 TCAGGCCGCAGGAAGAGGAA	This paper	N/A
mCherry-dyskerin Backbone forward TGAGAATTCTGCAGTCGACGG	This paper	N/A

mCherry-dyskerin Backbone reverse GTCGAGACTAGTACCTCCACC	This paper	N/A
mCherry-dyskerin insert forward GGAGGTACTAGTCTCGACATGGCGGATGCGGAAG	This paper	N/A
mCherry-dyskerin insert reverse GTCGACTGCAGAATTCTCACTCAGAAACCAATTCTA CCTCTTTTG	This paper	N/A
TR HRD Puro cassette forward GGATCCGGTGTGGAAAGTC	This paper	N/A
TR HRD Puro cassette reverse AAGCTTCACACAAAAAACCAACAC	This paper	N/A
3xFLAG-HaloTag-dysekrin Backbone forward TGAGCGGCCGCTTGCTG	This paper	N/A
3xFLAG-HaloTag-dysekrin Backbone reverse GGTACCGGAAGCGATCGC	This paper	N/A
3xFLAG-HaloTag-dysekrin insert forward ATCGCTTCCGGTACCATGGCGGATGCGGAAGTAAT T	This paper	N/A
3xFLAG-HaloTag-dysekrin insert reverse GCAAGCGGCCGCTCACTCAGAAACCAATTCTACCT CTTTTGC	This paper	N/A
3xFLAG-HaloTag-NLS iPCR forward GATGACGATGACAAGATAACTTCGTATAATGTATGC TATACGAAGTTATCCGGTACCATGGCAGAAATCGGT ACTGG	This paper	N/A
3xFLAG-HaloTag-NLS iPCR reverse CTTGTAATCGATATCATGATCTTTATAATCACCGTCA TGGTCTTTGTAGTCCATGGTGGCTTTGCTAGCCC	This paper	N/A
TR northern probe 1 CTTTTCCGCCCGCTGAAAGTCAGCGAG	Schmidt et al. 2018	N/A
TR northern probe 2 CTCCAGGCGGGGTTCGGGGGCTGGGCAG	Schmidt et al. 2018	N/A
TR northern probe 3 CGTGCACCCAGGACTCGGCTCACACATG	Schmidt et al. 2018	N/A
TR FISH Probe 1 /5Cy5/GCTGACATTTTTTGTTTGCTCTAGAATGAACG GTGGAAGGCGGCAGGCCGAGGCTT	Tomlinson *et al.* 2006	N/A
TR FISH Probe 2 /5Cy5/CTCCGTTCCTCTTCCTGCGGCCTGAAAGGCC TGAACCTCGCCCTCGCCCCCGAGAG	Tomlinson *et al.* 2006	N/A
TR FISH Probe 3 /5Cy5/ATGTGTGAGCCGAGTCCTGGGTGCACGTCCC ACAGCTCAGGGAATCGCGCCGCGCGC	Tomlinson *et al.* 2006	N/A
ACA57 FISH Probe 1 /5Cy5/ATTGCTGTGTGTCCTGCCAGACTACCCTGTTA G	This Paper	N/A
ACA57 FISH Probe 2 /5Cy5/ATTGTCCTCTCGTGCCTTTAAGAGCCAGCCCT ATTC	This Paper	N/A
TCAB1 locus primer F1 ctccttcacaacccttatcactc	This paper	N/A
TCAB1 locus primer F2 gagaacttcgaagccatcctg	This paper	N/A
TCAB1 locus primer R1 cagtcccgtttgtgaacagg	This paper	N/A

TR locus F ctgctcaaggagaggctgg	This paper	N/A
TR locus R ctcaaggtcatcgccaagg	This paper	N/A
TCAB1 southern probe forward gagaacttcgaagccatcctg	This paper	N/A
TCAB1 southern probe reverse cagtgaaaatctcgggggtgg	This paper	N/A
TR qPCR forward cgctgtttttctcgctgact	Xi et al. 2014	N/A
TR qPCR reverse gctctagaatgaacggtggaa	Xi et al. 2014	N/A
GAPDH qPCR forward acagcaacagggtggtggac	Xi et al. 2014	N/A
GAPDH qPCR reverse gaccattgctggggctggtg	Xi et al. 2014	N/A
Recombinant DNA		
pHTN HaloTag® CMV-neo	Promega	G7721
pFastBac1	Life Technologies	10360014
pX330	Cong et al., 2013	Addgene: 42230
pmaxGFP	Lonza	Control from Kits
mCherry-TERT	Schmidt et al. 2014	N/A to be deposited
TERT (pVAN107)	Cristofari et al. 2006	N/A
mCherry-Dyskerin	This paper	N/A to be deposited
3xFLAG-HaloTag-dyskerin	This paper	N/A to be deposited
pSUPER TR	Cristofari et al. 2006	N/A
TR knockout HRD	This paper	N/A to be deposited
Software and Algorithms		
MATLAB 2019a	Mathworks Inc., USA	http://mathworks.com
ParallelProcess_fastSPT_JF646.m	Hansen et al. 2018	https://github.com/elifesciences-publications/SPT_LocAndTrack
ImageQuant TL 8.2	Cytiva	cytivalifesciences.com
Spot-On	Hansen et al. 2018	https://github.com/elifesciences-publications/spot-on-matlab
Other		
SuperScript III	Invitrogen	18080044
Maxima SYBR Green qPCR Master Mix	Thermo Scientific	K0251
Random Hexamers	Invitrogen	N8080127
RiboLock RNase Inhibitor	Thermo Scientific	EO0382
Protein G Agarose	Millipore Sigma	11243233001
4-15% Mini-PROTEAN TGX precast protein gels	Bio-Rad	4561083
Trans-Blot Turbo RTA Mini 0.2 µm Nitrocellulose Kit	Bio-Rad	1704270